NASA/TM—2002-211127

Measurement and Computation of Supersonic Flow in a Lobed Diffuser-Mixer for Trapped Vortex Combustors

Andreja Brankovic and Robert C. Ryder, Jr.
Flow Parametrics, LLC, Bear, Delaware

Robert C. Hendricks, Nan-Suey Liu, and John R. Gallagher
Glenn Research Center, Cleveland, Ohio

Dale T. Shouse and W. Melvyn Roquemore
Wright-Patterson Air Force Base, Dayton, Ohio

Clayton S. Cooper and David L. Burrus
General Electric Aircraft Engines, Evendale, Ohio

John A. Hendricks
Diligent Design, Toledo, Ohio

The NASA STI Program Office . . . in Profile

Since its founding, NASA has been dedicated to the advancement of aeronautics and space science. The NASA Scientific and Technical Information (STI) Program Office plays a key part in helping NASA maintain this important role.

The NASA STI Program Office is operated by Langley Research Center, the Lead Center for NASA's scientific and technical information. The NASA STI Program Office provides access to the NASA STI Database, the largest collection of aeronautical and space science STI in the world. The Program Office is also NASA's institutional mechanism for disseminating the results of its research and development activities. These results are published by NASA in the NASA STI Report Series, which includes the following report types:

- TECHNICAL PUBLICATION. Reports of completed research or a major significant phase of research that present the results of NASA programs and include extensive data or theoretical analysis. Includes compilations of significant scientific and technical data and information deemed to be of continuing reference value. NASA's counterpart of peer-reviewed formal professional papers but has less stringent limitations on manuscript length and extent of graphic presentations.

- TECHNICAL MEMORANDUM. Scientific and technical findings that are preliminary or of specialized interest, e.g., quick release reports, working papers, and bibliographies that contain minimal annotation. Does not contain extensive analysis.

- CONTRACTOR REPORT. Scientific and technical findings by NASA-sponsored contractors and grantees.

- CONFERENCE PUBLICATION. Collected papers from scientific and technical conferences, symposia, seminars, or other meetings sponsored or cosponsored by NASA.

- SPECIAL PUBLICATION. Scientific, technical, or historical information from NASA programs, projects, and missions, often concerned with subjects having substantial public interest.

- TECHNICAL TRANSLATION. English-language translations of foreign scientific and technical material pertinent to NASA's mission.

Specialized services that complement the STI Program Office's diverse offerings include creating custom thesauri, building customized data bases, organizing and publishing research results . . . even providing videos.

For more information about the NASA STI Program Office, see the following:

- Access the NASA STI Program Home Page at *http://www.sti.nasa.gov*

- E-mail your question via the Internet to help@sti.nasa.gov

- Fax your question to the NASA Access Help Desk at 301–621–0134

- Telephone the NASA Access Help Desk at 301–621–0390

- Write to:
  NASA Access Help Desk
  NASA Center for AeroSpace Information
  7121 Standard Drive
  Hanover, MD 21076

NASA/TM—2002-211127

Measurement and Computation of Supersonic Flow in a Lobed Diffuser-Mixer for Trapped Vortex Combustors

Andreja Brankovic and Robert C. Ryder, Jr.
Flow Parametrics, LLC, Bear, Delaware

Robert C. Hendricks, Nan-Suey Liu, and John R. Gallagher
Glenn Research Center, Cleveland, Ohio

Dale T. Shouse and W. Melvyn Roquemore
Wright-Patterson Air Force Base, Dayton, Ohio

Clayton S. Cooper and David L. Burrus
General Electric Aircraft Engines, Evendale, Ohio

John A. Hendricks
Diligent Design, Toledo, Ohio

National Aeronautics and
Space Administration

Glenn Research Center

July 2002

Available from

Measurement and Computation of Supersonic Flow in a Lobed Diffuser-Mixer for Trapped Vortex Combustors

Andreja Brankovic and Robert C. Ryder, Jr.
Flow Parametrics, LLC
Bear, Delaware 19701

Robert C. Hendricks, Nan-Suey Liu, and John R. Gallagher
National Aeronautics and Space Administration
Glenn Research Center
Cleveland, Ohio 44135

Dale T. Shouse and W. Melvyn Roquemore
Wright-Patterson Air Force Base
Dayton, Ohio 45433

Clayton S. Cooper and David L. Burrus
General Electric Aircraft Engines
Evendale, Ohio 45215

John A. Hendricks
Diligent Design
Toledo, Ohio 43614

Summary

The trapped vortex combustor (TVC) pioneered by Air Force Research Laboratories (AFRL) is under consideration as an alternative to conventional gas turbine combustors. The TVC has demonstrated excellent operational characteristics such as high combustion efficiency, low NO_x emissions, effective flame stabilization, excellent high-altitude relight capability, and operation in the lean-burn or rich burn-quick quench-lean burn (RQL) modes of combustion. It also has excellent potential for lowering the engine combustor weight. This performance at low to moderate combustor mach numbers has stimulated interest in its ability to operate at higher combustion mach number, and for aerospace, this implies potentially higher flight mach numbers.

To this end, a lobed diffuser-mixer that enhances the fuel-air mixing in the TVC combustor core was designed and evaluated, with special attention paid to the potential shock system entering the combustor core.

For the present investigation, the lobed diffuser-mixer combustor rig is in a full annular configuration featuring sixfold symmetry among the lobes, symmetry within each lobe, and plain parallel, symmetric incident flow. During hardware cold-flow testing, significant discrepancies were found between computed and measured values for the pitot-probe-averaged static pressure profiles at the lobe exit plane. Computational fluid dynamics (CFD) simulations were initiated to determine whether the static pressure probe was causing high local flow-field disturbances in the supersonic flow exiting the diffuser-mixer and whether shock wave impingement on the pitot probe tip, pressure ports, or surface was the cause of the discrepancies. Simulations were performed with and without the pitot probe present in the modeling.

A comparison of static pressure profiles without the probe showed that static pressure was off by nearly a factor of 2 over much of the radial profile, even when taking into account potential axial displacement of the probe by up to 0.25 in. (0.64 cm). Including the pitot probe in the CFD modeling and

data interpretation lead to good agreement between measurement and prediction. Graphical inspection of the results showed that the shock waves impinging on the probe surface were highly nonuniform, with static pressure varying circumferentially among the pressure ports by over 10 percent in some cases.

As part of the measurement methodology, such measurements should be routinely supplemented with CFD analyses that include the pitot probe as part of the flow-path geometry.

Introduction

The trapped vortex combustor (TVC) is being considered as an alternative to conventional gas turbine combustors. The TVC pioneered by Air Force Research Laboratories (AFRL) (refs. 1 to 3) represents a relatively simple and highly advantageous alternative to conventional swirl-stabilized combustors. Hardware photographs, combustion flow-visualization images, and detailed performance plots for NO_x emissions, lean blowout, and combustion efficiency are presented in detail in references 1 and 2 and to some extent in reference 3. Also discussed are fluid dynamics and combustion physics for a baseline TVC that is operating under different fueling conditions at subsonic combustor core flows, presented with the aid of computational fluid dynamics (CFD) images of the flow-field aerodynamics and combustion process.

The outstanding performance at low to moderate combustor mach numbers has stimulated interest in its ability to operate at higher combustion mach number, which for aerospace applications implies potentially higher flight mach numbers.

At the lower combustor mach numbers the TVC has demonstrated excellent operational characteristics such as high combustion efficiency, low NO_x emissions, effective flame stabilization, excellent high-altitude relight capability, and operation in the lean-burn or rich burn-quick quench-lean burn (RQL) modes of combustion. It also has excellent potential for lowering the engine combustor weight.

To preserve these characteristics when designing a new combustor for operation in a higher mach number flow regime, special attention must be paid to the combustor diffusion system and to understanding the physics of the potential shock system entering the combustor core. This was accomplished by evaluating the flow through the lobed diffuser-mixer into the TVC annulus, which enhances the fuel-air mixing in the TVC combustor core.

For the present investigation, the combustor rig is in a full annular configuration as opposed to the planar configuration of references 1 to 3. The computer-aided design (CAD) solid model of the full annular combustor with a lobed diffuser-mixer is shown in figure 1(a), with a view looking downstream. The experimental combustor geometry consists of a short, straight inlet pipe, lobed transition duct, trapped vortex annulus with fuel and air injector ports facing upstream, and a circular combustor duct downstream of the core. This design features sixfold symmetry so that CFD analyses modeled only a 60° sector to capture all the relevant flow physics, assuming the incident flow is also symmetric.

During the evaluation stage, significant discrepancies were found between the computed and the measured average static pressure profiles at the lobe exit plane. The present work was initiated during hardware cold-flow testing to determine whether the static pressure probe was causing high local flow-field disturbances in the supersonic flow exiting the diffuser-mixer and whether shock wave impingement on the pitot probe tip, pressure ports, or surface was the cause of the discrepancies between computations and measurements.

CFD simulations of air flow in the lobed duct system were performed with and without the pitot probe present in the modeling. The pitot probe configuration was introduced into the computational model through a full CAD solid model representation and was inserted and traversed consistently with the experimental sampling method.

A comparison of experimental and CFD static pressure profiles without including the probe in the model showed that the CFD static pressure was off by nearly a factor of 2 over much of the radial profile, even when taking into account potential axial displacement of the probe by up to 0.25 in. (0.64 cm).
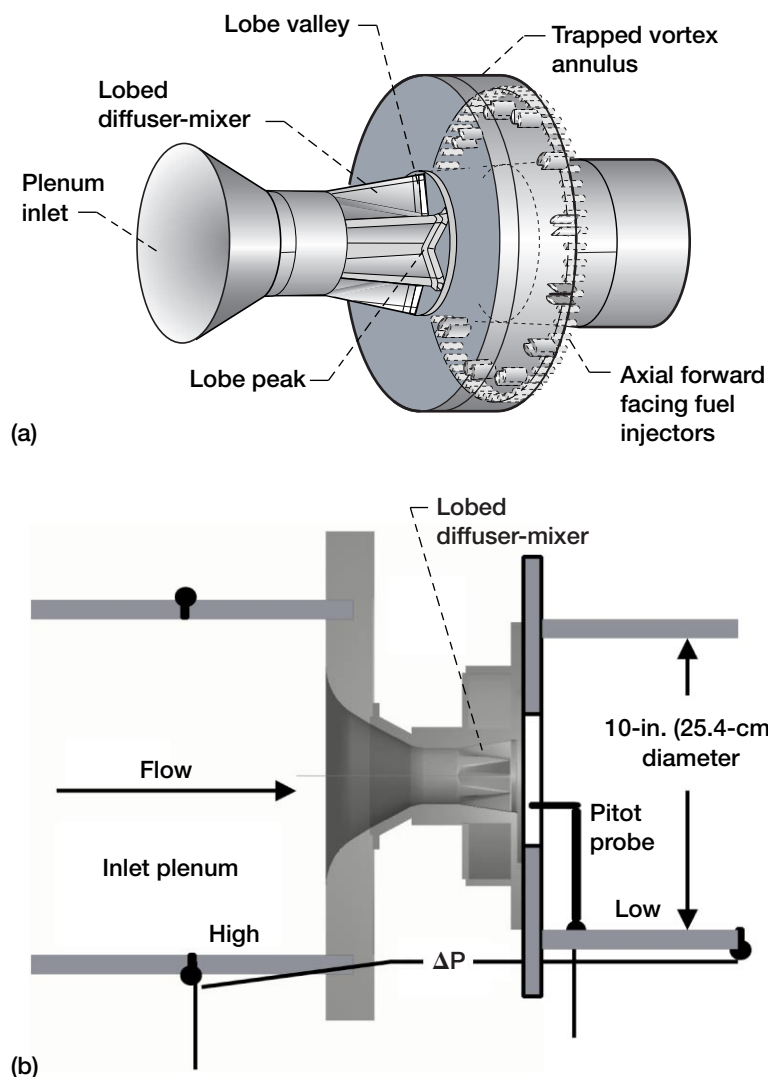
Figure 1.—Trapped vortex combustor (TVC) with lobed diffuser-mixer.
Fueling concept features axial forward and rearward facing injectors.
(a) CAD solid model. (b) Test section schematic.

The pitot probe was then included in the CFD modeling and data interpretation, and good agreement between measurement and prediction was achieved. Graphical inspection of the results showed that the shock waves impinging on the probe surface were highly nonuniform, with static pressure varying circumferentially among the pressure ports by over 10 percent in some cases.

The CFD simulations demonstrated that pitot probe pressure measurements in supersonic flow regions must be interpreted with care because of significant local flow-field disturbances and their impact on the measured result. Averaging the four static pressures clocked 90° about the pitot probe introduces significant errors and is inadequate as opposed to individual sampling. Also, probe incidence angle and sting strain require consideration. As part of the measurement methodology, such measurements should be routinely supplemented with CFD analyses that include the pitot probe as part of the flow-path geometry.

The appendix presents supplementary results for flow through a lobed diffuser-mixer that illustrate the relevant fluid dynamics effects of a pitot probe in the flow path.

Lobed Diffuser-Mixer Cold-Flow Test

The cold-flow test hardware consisted of the upstream nozzle and the lobed diffuser-mixer that projected into a pipe that was 10 in. (25.4 cm) in diameter and 39 in. (100 cm) long. The TVC cavity annulus was not part of the test, and the pipe exhausted to the atmosphere (fig. (1b)). The working fluid was air.

CFD Codes and Conditions

The flow solver selected for this work was the commercially available, second-generation version of the NASA Glenn Research Center (GRC) National Combustion Code (NCC) called FPVortex that was developed by Flow Parametrics, LLC (Bear, Delaware). The approach of Ryder and McDivitt (ref. 4) is followed to model the test rig hardware as installed on the test stand. In this analysis, the pitot probe was incorporated in the existing lobed duct CAD solid model, and new computational grids were generated for each of the six probe positions modeled.

The resulting grid is transferred to an unstructured geometry data base and read in by the flow solver. Intermediate results data bases are created and can be viewed automatically in graphics postprocessing packages. The physics-based modeling for the aerodynamic simulations includes the two-equation k-ε model of turbulence with wall functions.

The inlet boundary condition consists of the subsonic airflow conditions (velocity and mass flow rate), which feed the inlet plenum. The inlet static pressure for these cases was 50 psia (345 kPaa). The exit boundary condition simulated the laboratory pressure condition; the flow at the pipe exit was vented into the room at a nominal atmospheric pressure of 14.7 psia (101 kPaa). At high flow rates, the flow chokes at the minimum-area location at the exit and forms a shock pattern, which extends well into the downstream duct, eventually dissipates, and changes back to subsonic flow.

High-Speed Flow Structure

A CFD simulation of the aerodynamics of flow through the lobed duct diffuser-mixer was run to gain an understanding of the main flow features in the device. Mach number contour plots of the flow from the lobe into the large-diameter pipe are shown in figure 2, illustrating the flow complexity in that region. A supersonic jet core penetrates well into the combustor core and remains supersonic for a length of about five lobe heights downstream of the lobe exit plane. The supersonic core transforms from a lobe-shaped cross section to a circular shape over a length of about two lobe heights as it moves downstream. High-speed, discrete cellular structures are clearly present, forming a shock train with five to six distinct cells. Clearly visible at the lobed duct exit plane are regions of high-velocity and high-pressure gradients as the flow expands from subsonic to supersonic. This is the region in which pressure profiles were taken using a pitot pressure probe constructed for use in this test rig.

Pitot Pressure Probe

The performance characteristics of the lobed duct were measured to assess the effectiveness of the design. Measurements included pressure loss and radial profiles of total and static pressure at the lobed duct exit plane. To accomplish this, a pitot probe with multiple static openings (ref. 5) was designed and mated to a traversing mechanism attached to the outer duct. The probe was moved radially in line with either the lobe peaks or troughs (which were clocked at 30°). A schematic diagram of the probe is shown in figure 3. The frontal portion of the probe had a 0.125-in. (0.3175-cm) diameter and was turned to face upstream into the flow. Using pressure transducers, the pitot tube directly measures total pressure P_T at
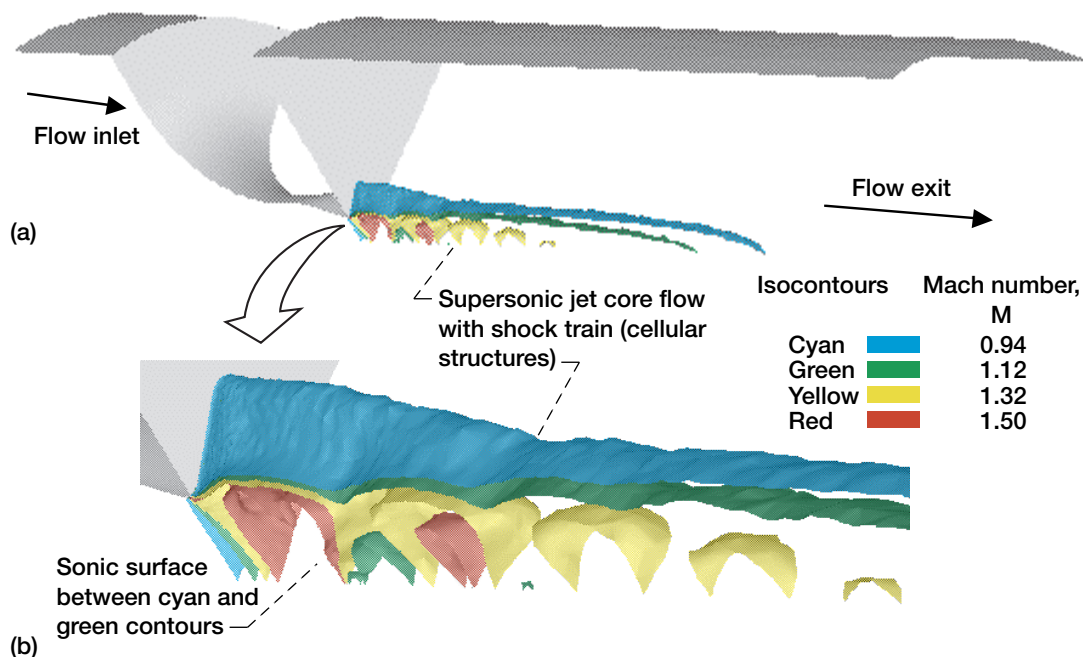
Figure 2.—Supersonic flow structure downstream of the lobed diffuser-mixer exit plane.
(a) Overall length of the supersonic core flow. (b) Detail of the cellular structure in the core.

the probe tip and static pressure P_S at four ports clocked at 90° about the circumference and 0.50 in. (1.27 cm) downstream of the tip. Accuracy issues include providing tubing with adequate frequency response, calibration, and pitch-yaw sensitivity to the flow direction.

In the supersonic flow case, the accuracy of pitot tubes is more questionable mainly because of the presence of shock waves that may intersect the probe normally or at oblique angles and also because of high-velocity gradients and stability of small-scale flow features, which may easily be disturbed by the presence of the probe.

The data comparisons shown in figures 4 and 5 illustrate pitot probe accuracy issues for supersonic flow. In figure 4, radial profiles of total pressure are shown from the duct centerline to the lobe valley (fig. 4(a)) and from the duct centerline to the lobe peak (fig. 4(b)). Because the total pressure is measured at the probe tip, there is minimal local flow disturbance, and excellent agreement between experimental data and CFD predictions can be seen. The relevant profiles are at axial position Z, which represents the plane in which the radial profiles are measured. Additional curves sampled from the CFD simulations are shown at downstream locations, establishing the trend in axial variation of total pressure. Thus, for total pressure it appears that in spite of the potential for shock waves and other high-gradient flow structures, the pitot probe is adequate for capturing the quantitative total pressure profiles for the lobed diffuser-mixer at high-speed operation.
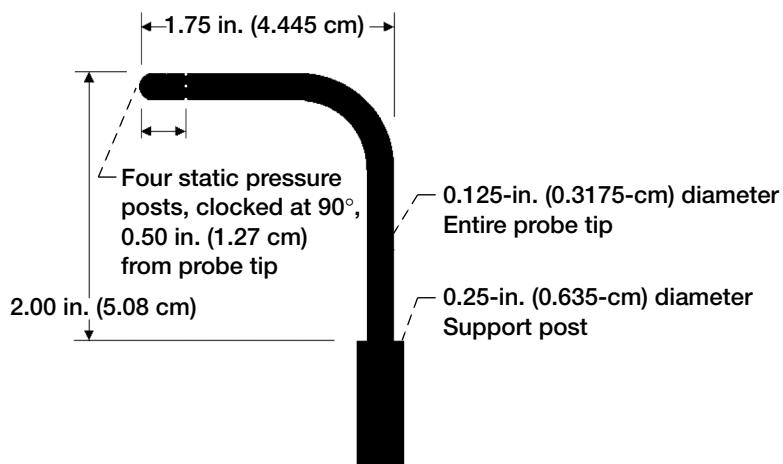

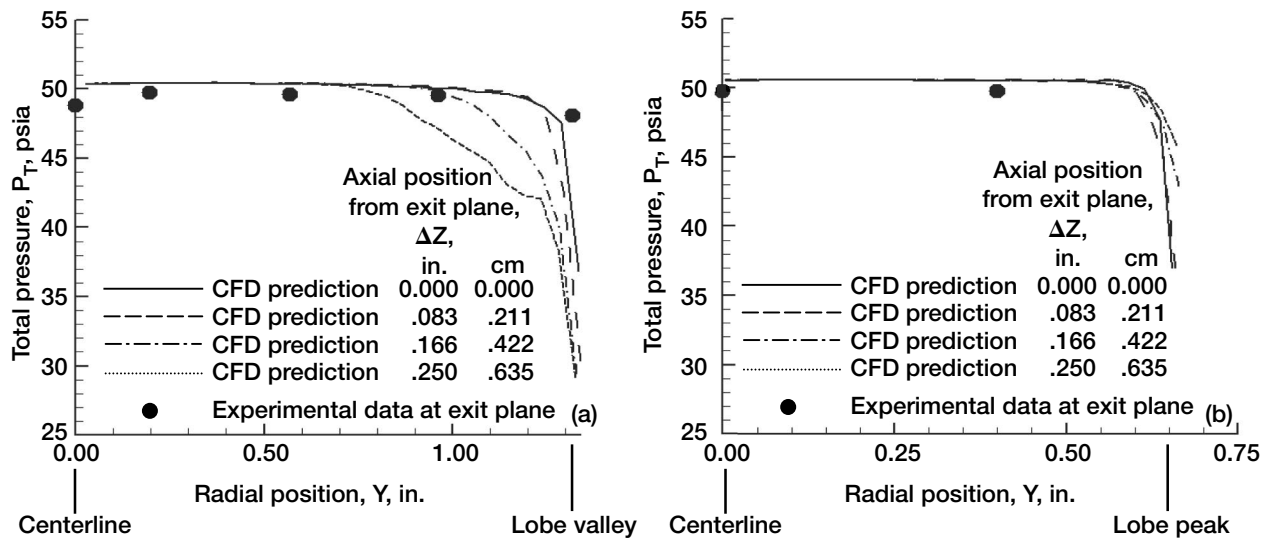Figure 3.—Pitot pressure probe used to measure radial profiles in downstream pipe.

Figure 4.—Comparisons of experimental and CFD simulation static pressure P_T profiles for baseline case without pitot probe in model. (a) Profiles from duct centerline to lobe valley. (b) Profiles from duct centerline to lobe peak, 30° off axis.
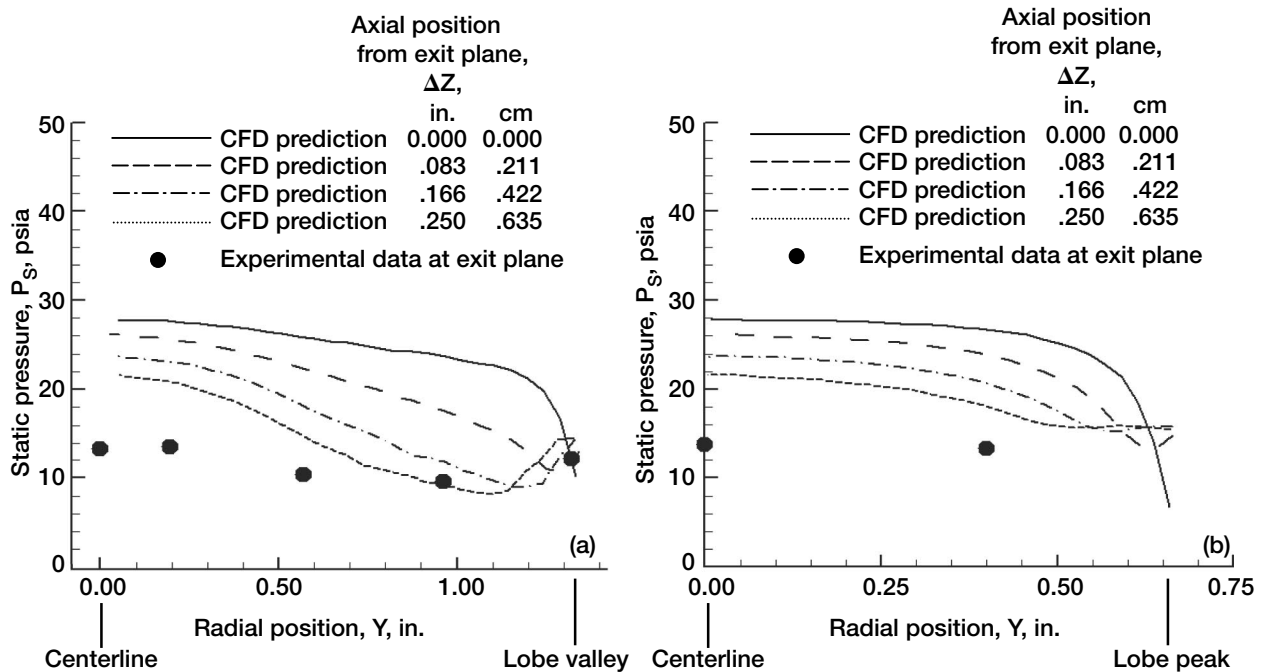

Figure 5.—Comparisons of experimental and CFD simulation static pressure P_S profiles for baseline case without pitot probe in model. Static pressure ports are located 0.50 in. (1.27 cm) downstream of probe tip. (a) Profiles from duct centerline to lobe valley. (b) Profiles from duct centerline to lobe peak, 30° off axis.

The major problem with the correlation between the experimental and CFD data is in the interpretation of the radial profiles of static pressure, measured using the same pitot probe. Comparisons of experimental data and CFD simulations are shown in figure 5 and demonstrate discrepancies of a factor of 2 or more between measured and computed values of P_S, even at the duct centerline. This was also the case even for CFD simulations taken at axial positions further downstream in the duct, corresponding to the axial location of the static pressure ports 0.50 in. (1.27 cm) downstream of the probe tip, as seen in figure 3.

Initial attempts to resolve these discrepancies included rechecking the pressure transducer calibration technique and values as well as the simulation boundary conditions. However, no significant errors were discovered. To further investigate these discrepancies, it was decided to proceed with a more detailed CFD study and to include the presence of the pitot probe in the flow simulations.

Lobe and Pitot Flow Description

Because of the large discrepancy in static pressure profiles between experimental data and CFD simulations observed and discussed in the previous section, the CFD analysis of the duct was repeated with the pitot probe included in the computational model.

The results of these simulations are shown graphically through contour plots in figures 6 and 7, which illustrate the flow-field distortion in the vicinity of the probe tip and the static pressure ports caused by the pitot probe in the presence of the high-velocity and high-pressure gradients. Axial cross sections of three of the six simulations are shown in figure 6, for static pressure and mach number. The baseline flow without the probe is shown at the top, whereas flows with the probe at radial positions 0.60 in. (1.5 cm) and 1.30 in. (3.3 cm) are shown immediately below. The flow region shown represents only the near field of the lobed duct exit plane and probe tip. The overall computational model used in the updated simulations was the same as that used to generate figure 2.

It is observed in figure 6 that the pitot probe tip is relatively unaffected by the shock formed at the lobed duct exit plane lip, explaining why the total pressure profiles are in good agreement with the data, even with the nearby shock system. The shock instead impinges on the probe stem and wraps around it, which results in large pressure and mach number gradients axially down the stem of the probe. (Circumferential variations in pressure could have been monitored if the four clocked static ports had individual readouts. If individual stings or a wedge probe were used, the flow angle could have been monitored; however, the probe used in this analysis had a common port, providing a uniform static pressure.)

The effect of the shock system is further illustrated in figure 7, which shows axial cuts of the flow field in the plane of the pitot probe pressure ports 0.50 in. (1.27 cm) downstream of the probe tip. In addition to the axial gradient along the stem noted above, there is a strong circumferential gradient of static pressure and mach number about the probe, which differs substantially from one probe position to the next. The impact of the probe on the local flow field is clearly visible in these figures. At radial position Y = 0.60 in. (1.5 cm), the probe attracts the low static pressure region of flow in the lobe, causing a deformation of the pressure field. At radial position Y = 1.30 in. (3.3 cm) off the centerline, the probe distorts the flow issuing from the probe valley, forcing a type of bifurcation substantially from one probe position to the next. The impact of the probe on the local flow field is seen clearly in the flow and in the shifting of the low-pressure region inward toward the duct centerline.

These flow simulations strongly suggest that the shock wave impingement, high-velocity and high-pressure gradient flow, and the local flow disturbance due to the pitot pressure probe cumulatively contribute to the discrepancies observed in the computed and measured radial profiles of static pressure shown in figure 5. Such discrepancies would even be found for the case of uniform flows if one were seeking pressure distributions downstream of the probe (fig. 8). These pitot probe accuracy issues do not arise in low-speed, incompressible flows because of the absence of compressibility effects.
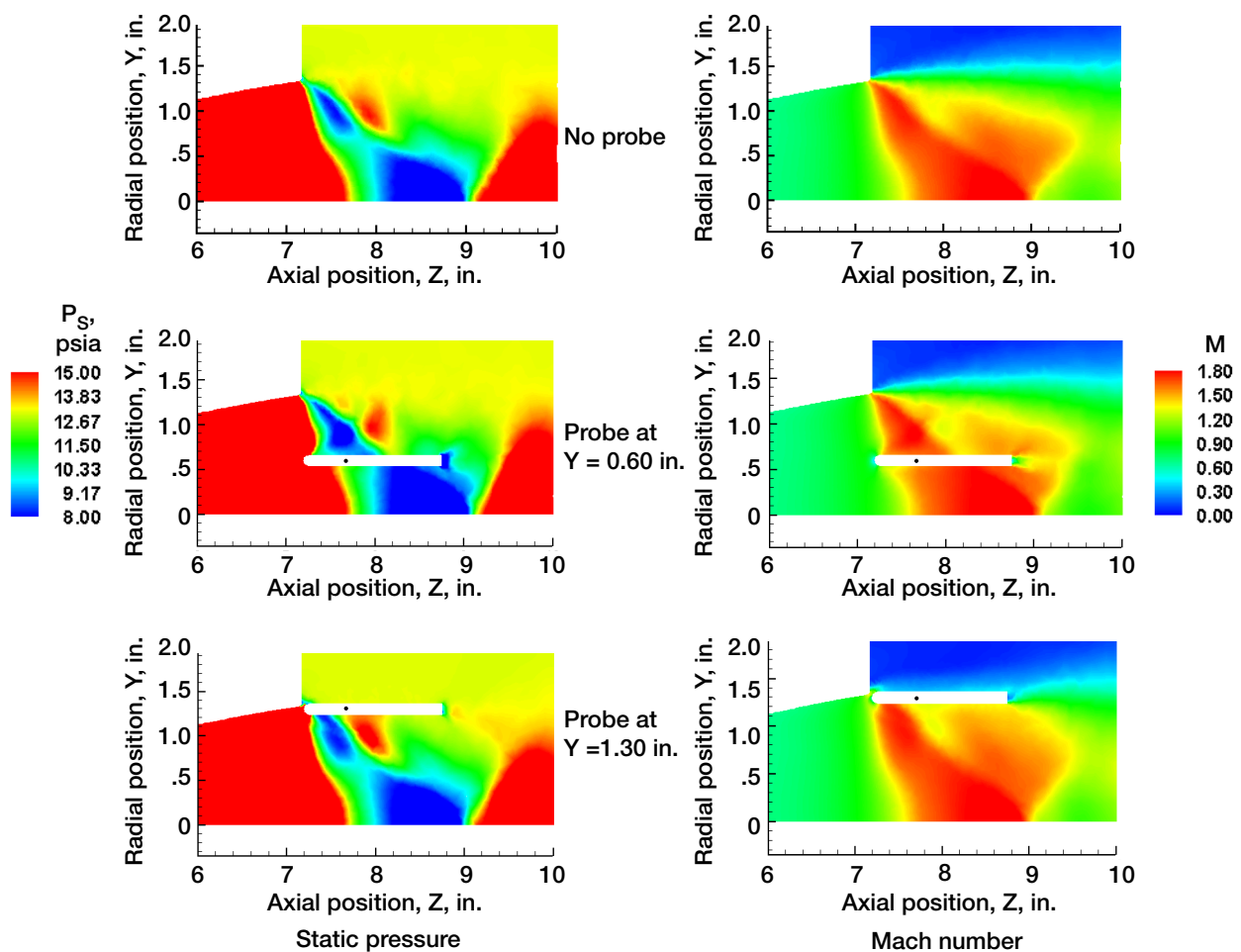
Figure 6.—Flow-field distortions in static pressure P_S and mach number M distributions for three of six CFD simulations. Top row: baseline flow field without probe. Middle row: probe at 0.60 in. (1.52 cm) off duct centerline. Bottom row: probe at 1.30 in. (3.30 cm) off duct centerline.
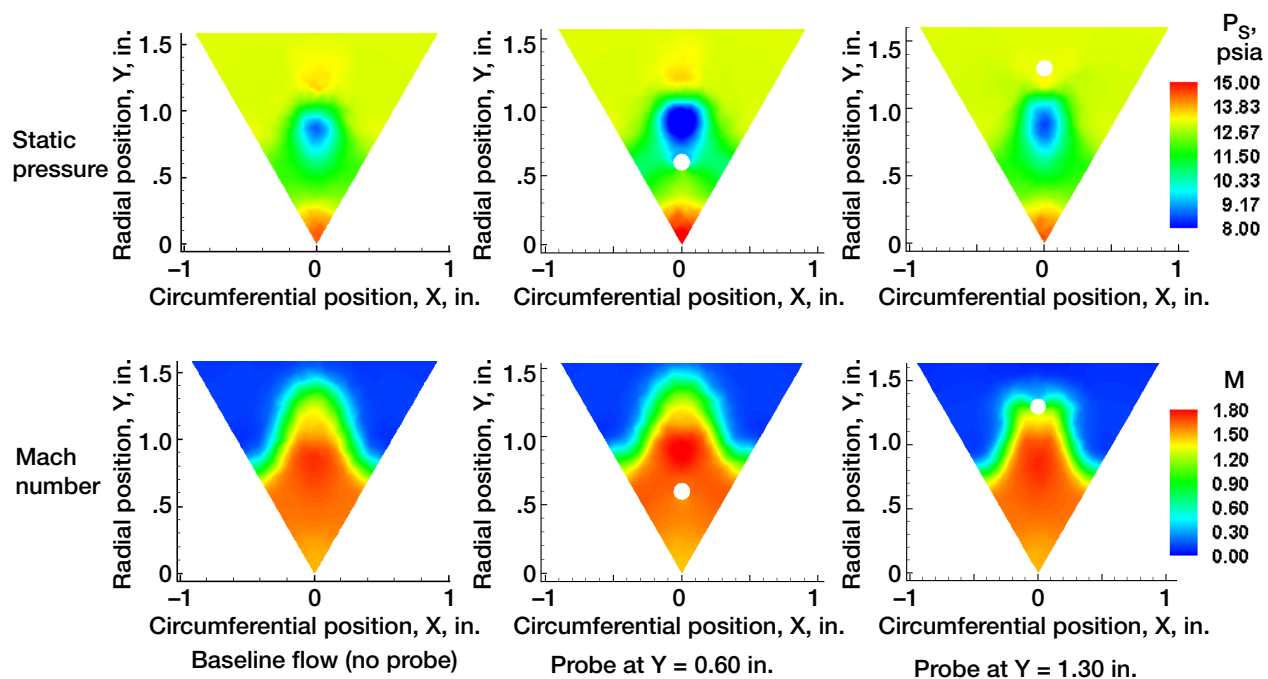
Figure 7.—Axial slices in plane of pitot-static pressure ports, 0.50 in. (1.27 cm) downstream of probe tip, for three of six CFD simulations. Top row: static pressure P_S distributions. Bottom row: mach number M distributions.

Figure 8.—Pitot probe and support shock structure interaction.

With this knowledge, CFD simulations with the pitot probe in six unique positions were run, post-processed, and compared again with the radial profiles of static pressure.

Comparison of Experimental Data With CFD Predictions

With the new understanding gained from the analysis of the flow-field distortions caused by the pitot probe, the six CFD simulations that included the probe were further sampled and compared with the experimental data.

Total Pressure Profile Results

Although predicted total pressure profiles were already considered to be in good agreement with experimental data, the results were replotted using the probe tip as the sampling point. These results are shown in figure 9 in the form of a radial total pressure profile aligned tangentially with the lobe valley at its highest radius. Both the predictions and experimental data show a relatively flat radial profile across the duct at a level of about 50 psia (345 kPaa) (inlet pressure specification). Note that discrete data points and simulation points are now being plotted because the presence of the probe affects the flow field differently at each unique location. Thus, with the probe causing large local disturbances, it is no longer assumed that line profiles can be extracted from a single CFD simulation and be compared with data.

For the simulation with the probe at a radial position of $Y = 1.30$ in. (3.3 cm), the CFD predictions fall off slightly from the experimental value. It was observed in the CFD line profiles in figure 4 that there was a rapid dropoff in the total pressure at positions further axially downstream. This pressure drop can be appreciated to some extent in the contour plots in figures 6 and 7, which show the pitot probe facing into the lobe wall boundary layer, with high-speed flow on the lower probe surface and low-speed flow on the upper surface. Under this condition, which features extreme pressure and velocity gradients, any variance in either the radial or axial positioning of the probe can result in large variation in the sampled
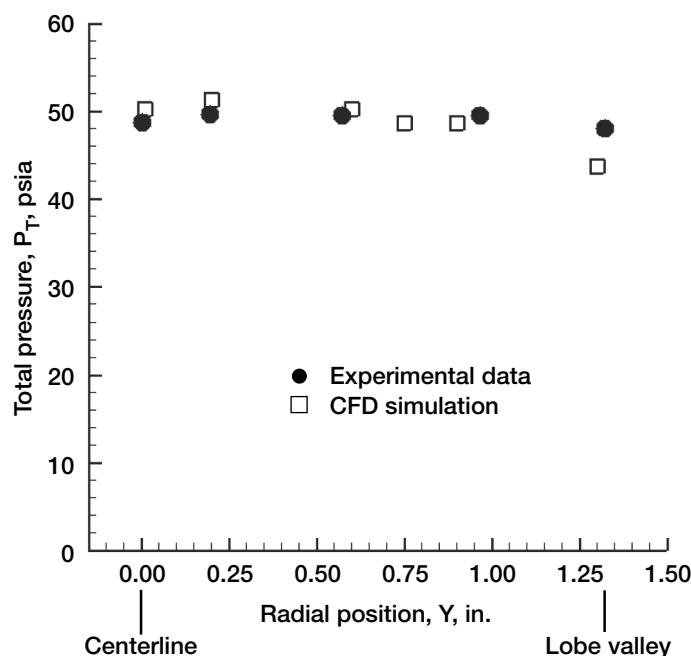
Figure 9.—Comparison of experimental and CFD simulation total pressure P_T profiles with pitot probe in model. CFD data points sampled at probe tip.

pressure. Thus, it is concluded that because of the proximity of the probe to the lobe exit plane and its position within the duct boundary layer, this particular data point is subject to higher uncertainty than data points taken with the probe in the free-stream positions away from the duct wall.

Static Pressure Profile Results

The key results of comparisons between the static pressure measurements and CFD analysis appear in figure 10, which presents radial profiles of measured and predicted static pressures that include the presence of the pitot probe. The overall agreement between experimental data and CFD simulations is good and is much better than that observed without including the probe (fig. 5). Once again, discrete experimental data points and discrete CFD simulation points are compared because the probe affects the local flow field differently at each probe position. At the duct centerline (see fig. 10), excellent agreement between measurement and prediction is observed. This agreement was expected, because the CFD computational model, taken to be a symmetric 60° sector, models the flow blockage from a pipe (in this case, a pitot pressure probe) situated at the centerline.

As the probe is moved radially outboard, there is a discrepancy in the comparison at a radial position of $Y = 0.20$ in. (0.5 cm) off the duct centerline. The interpretation of this result is that with a symmetric model of the duct, insertion of a single probe is the physical equivalent of inserting six probes into the domain and accounts for the same percentage of flow blockage in that area. The symmetry modeling condition thus forces an unrealistic flow blockage to occur in the duct, with resulting questionable to poor agreement in the results. Further outboard, the agreement between predictions and measurements is very good. Although the flow model is still symmetric, as the probe moves deeper into the lobed duct valley, the interaction with the actual probe and modeled symmetry probes becomes negligible, and the probe correctly models the local flow disturbances. This agreement extends to the furthest radial point measured
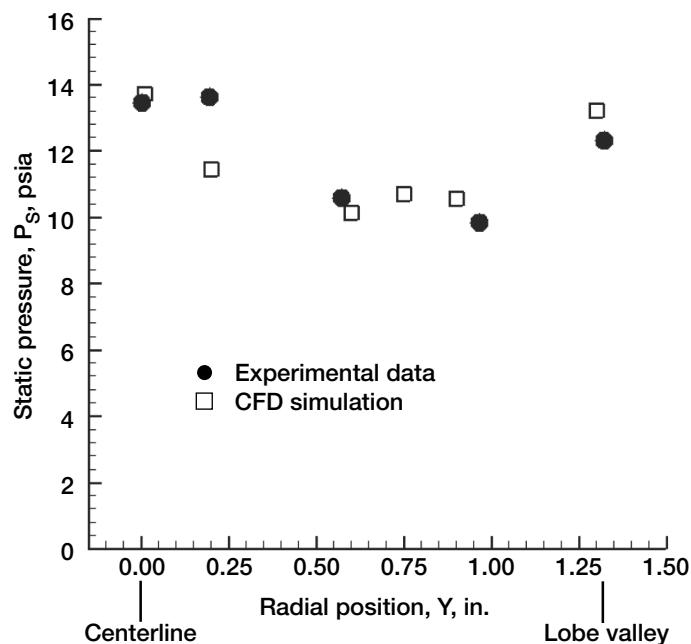

Figure 10.—Comparison of experimental and CFD simulation static pressure P_S profiles with pitot probe in model. CFD data points taken 0.50 in. (1.27 cm) downstream of probe tip and circumferentially averaged.

to position $Y = 1.30$ in. (3.3 cm), where the static pressure ports are exposed to a complex flow field ranging from low-speed subsonic flow on the ports facing the outer duct wall to high-speed supersonic flow at about mach 1.8 on the pressure ports facing the duct centerline.

Modeling of the pitot probe for this supersonic flow appears to be necessary to interpret the experimental pressure measurements. Although probe-induced flow interference is a necessity in many complex and high-speed applications in which optical and other nonintrusive measurements may be applied, the local flow disturbances observed in these supersonic aerodynamic measurements were very large and could not easily be interpreted without the benefit of the CFD modeling. For good agreement across the entire duct cross section, it is likely necessary to model the full 360° of the duct to avoid the probe blockage effect described above.

Effective Area Analysis

For use in flight, the lobed duct must have a low area discharge coefficient (AC_D) loss. Analysis of the CAD solid model of the lobed duct indicates that the cross-sectional area is equal to 2.748 in.^{2} (17.73 cm^2) along the 0.25-in. (0.64-cm) straight length just upstream of the lobe exit plane. The lobed duct area is equal to 3.08 in.^{2} (19.87 cm^2) at the lobe exit plane and includes the area increase due to a 0.09-in.- (0.24-cm-) radius lip along the edge of the lobe exit.

Computing the duct effective area in compressible, transonic flow introduces complications in the data reduction process, particularly those involving measurements taken with the pitot probe. Two experimental cold-flow measurements of the lobed duct parameter AC_D were performed. The first used an aluminum prototype lobed duct on an incompressible water table and gave $AC_D = 2.35$ in.^{2} (15.16 cm^2). The second, a compressible blowdown air test, used the stainless steel experimental lobe only, discharged into the 10-in. (25.4-cm.) duct, and gave $AC_D = 2.57$ in.^{2} (16.58 cm^2). For the lobe-TVC assembly, a hot-flow (reacting) test resulted in a value of 2.90 in.^{2} (18.71 cm^2). The experimental AC_D is calculated from the measured mass flow rate and the pressure differential between the plenum and the duct static pressure DP (fig. 1(b)). The density is evaluated at the upstream plenum conditions.

CFD simulations produced a value of $AC_D = 3.05$ in.^{2} (19.68 cm^2) when corrected for compressibility effects but produced only 1.65 in.^{2} (10.64 cm^2) when not corrected. With compressibility effects taken into account, the lobed duct appears to have a very high discharge coefficient C_D of approximately 0.99, which is an acceptable value for use in flight hardware applications.

Concluding Remarks

This report described an experimental and computational investigation aimed at understanding diffuser-mixer exit profiles for a lobed duct design that will potentially be used for higher mach number combustion evaluations of the trapped vortex combustor (TVC). Experimental hardware was described by using CAD solid models to show the major flow features present in this diffuser-mixer combustor system. Initial CFD simulations were compared with experimental data and showed good agreement with total pressure measurements but poor agreement with static pressure measurements, all of which were taken with a single simple pitot pressure probe sampling one sector of the lobe configuration. Even when considering axial and radial variations in positioning of either the probe or the CFD sampling plane, checking the pressure transducer calibrations, and verifying the CFD boundary conditions, poor agreement remained.

The CFD modeling methodology was modified to take into account the presence of the pitot probe, and the simulations were rerun. Flow-field contours of static pressure and mach number in the vicinity of the probe verified that the probe caused large, local disturbances. The graphics also showed that large

axial, radial, and tangential velocity and pressure gradients near the static pressure ports were acting on the probe and were reflected in the experimental data points.

With the probe included in the CFD model, six new simulations were run with the probe moved through the model as in the experiment. These results were very encouraging in that the established good agreement between measured and computed values for total pressure was repeated under the new methodology, and static pressure profiles were also now in good agreement.

Measurements taken at a radial position 0.20 in. (0.5 cm) off the duct centerline were in poor agreement with predictions. This result was attributed to the symmetry modeling condition assumed for the CFD simulations: at a position close to the centerline, the effect of a network of six probes was to cause a flow blockage (modeling artifact). This effect was negligible at larger radial positions where good agreement between data and predictions was achieved. Especially impressive was agreement at a radial position where the probe straddled the boundary layer–shear layer coming off the lobe valley. At this position, the probe upper surface faced low-speed (subsonic) flow conditions, whereas the probe lower surface faced the duct centerline and experienced an attached shock wave with a speed exceeding mach 1.7. Circumferential averaging of the CFD predicted static pressures at the four pressure ports resulted in excellent agreement with data.

It is concluded that with the CFD simulation results, the pressure measurements in the lobed diffuser-mixer are more accurately interpreted, and the pressure performance of the duct is better understood so that design improvement of the lobed diffuser-mixer system can proceed with more confidence.

Appendix—High-Speed Aerodynamic Results for Flow Through a Lobed Diffuser-Mixer Duct Issuing Into a Large Diameter Circular Pipe

   Herein are supplementary charts from the CFD study of the effects of a pitot pressure probe in the supersonic flow path. These CFD results provided the initial proof that the pressure probe was interacting with the flow and suggest that at least the probe tip should be modeled in any duct flow cases involving supersonic and transonic flows. In many cases the support sting also requires modeling as bow shocks, shock interaction loadings, and probe angle of attack can interfere with the measurements and cause distortions (see fig. 8).
   Each of the supplemental figures is titled and largely self-explanatory when viewed as supplementary to the body of the report. Consequently, only a brief statement relative to each figure will be given.
   • Figure 11 gives the geometric parameters associated with the test section (see fig. 1).
   • Figures 12 and 13 provide more details of the local shock patterns associated with the lobed diffuser-mixer configuration and provide additional details supporting figure 2.
   • Figures 14 and 15 show the static pressure contours at the exit plane and 0.5 in. downstream at the four-hole static location on the pitot probe (see also fig. 7).
   • Figures 16 and 17 show the total pressure contours at the exit plane and 0.5 in. downstream at the four-hole static location on the pitot probe.
   • Figures 18 and 19 give the local mach number contours at the exit plane and 0.5 in. downstream at the four-hole static location on the pitot probe (see also fig. 7).
   • Figure 20 represents the axial variations in static pressure along the lobed diffuser-mixer valley (see figs. 1 and 11) without the pitot probe in the flow field.
   • Figure 21 represents the axial variations in static pressure along the lobed diffuser-mixer valley (see figs. 1 and 11) with the pitot probe at the centerline of the flow field.
   • Figure 22 gives the static pressure contours for the pitot probe at 0.75 in. from the flow centerline (compare with fig. 6).
   • Figure 23 represents the axial variations in total pressure along the lobed diffuser-mixer valley (see figs. 1 and 11) without the pitot probe in the flow field.
   • Figure 24 represents the axial variations in total pressure along the lobed diffuser-mixer valley (see figs. 1 and 11) with the pitot probe at the centerline of the flow field.
   • Figure 25 gives the total pressure contours for the pitot probe at 0.75 in. from the flow centerline.
   • Figure 26 represents the axial variations in mach number along the lobed diffuser-mixer valley (see figs. 1 and 11) without the pitot probe in the flow field.
   • Figure 27 represents the axial variations in mach number along the lobed diffuser-mixer valley (see figs. 1 and 11) with the pitot probe at the centerline of the flow field.
   • Figure 28 gives mach number contours for the pitot probe at 0.75 in. from the flow centerline (compare with fig. 6).
   • Figure 29 gives axial slices in static pressure for the lobed diffuser-mixer (see figs. 1 and 11) without the pitot probe in the flow field to 1.5 in. downstream of the exit plane (see also fig. 7).
   • Figure 30 gives axial slices in total pressure for the lobed diffuser-mixer (see figs. 1 and 11) without the pitot probe in the flow field to 1.5 in. downstream of the exit plane.
   • Figure 31 gives axial slices in mach number for the lobed diffuser-mixer (see figs. 1 and 11) without the pitot probe in the flow field to 1.5 in. downstream of the exit plane (see also fig. 7).
   • Figure 32 gives axial slices in static pressure for the lobed diffuser-mixer (see figs. 1 and 11) with the pitot probe in the flow field to 1.5 in. downstream of the exit plane (see also fig. 7).
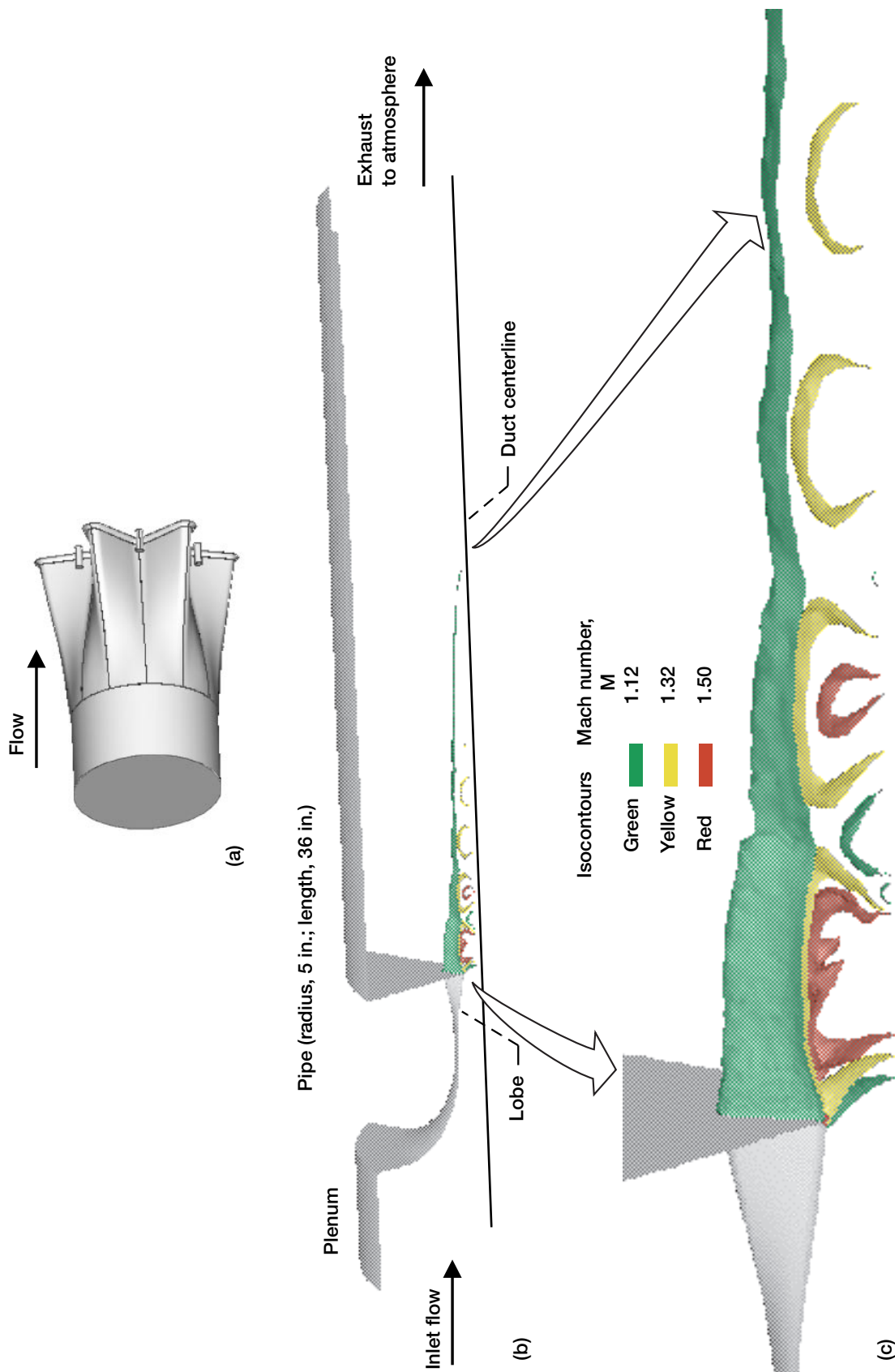   • Figure 33 gives axial slices in total pressure for the lobed diffuser-mixer (see figs. 1 and 11) with the pitot probe in the flow field to 1.5 in. downstream of the exit plane.
   • Figure 34 gives axial slices in mach number for the lobed diffuser-mixer (see figs. 1 and 11) with the pitot probe at the flow centerline to 1.5 in. downstream of the exit plane (see also fig. 7).

• Figure 35 gives axial slices in static pressure for the lobed diffuser-mixer (see figs. 1 and 11) with the pitot probe in the lobe valley to 1.5 in. downstream of the exit plane (see also figure 7).

• Figure 36 gives axial slices in total pressure for the lobed diffuser-mixer (see figs. 1 and 11) with the pitot probe in the lobe valley to 1.5 in. downstream of the exit plane.

• Figure 37 gives axial slices in mach number for the lobed diffuser-mixer (see figs. 1 and 11) with the pitot probe in the lobe valley to 1.5 in. downstream of the exit plane (see also fig. 7).

(a)

Flow

Pipe (radius, 5 in.; length, 36 in.)

Exhaust to atmosphere

Duct centerline

Plenum

Inlet flow

Lobe

(b)

Isocontours | Mach number, M
Green | 1.12
Yellow | 1.32
Red | 1.50

(c)

Figure 11.—Test section geometric parameters and three-dimensional cellular shock structure downstream as lobe expands into straight pipe. (a) Lobed diffuser-mixer geometry. (b) Overall view. (c) Local details of cellular shock structure.

Flow direction

Flow direction

Lobe

(a)

Shock assumes lobe
shape initially

Shock rapidly reverts
to circular shape

Isocontour   Mach number,
              M

Yellow   1.32

Red   1.50

Shock train rapidly
transforms from lobe
shape to circular shape

(b)
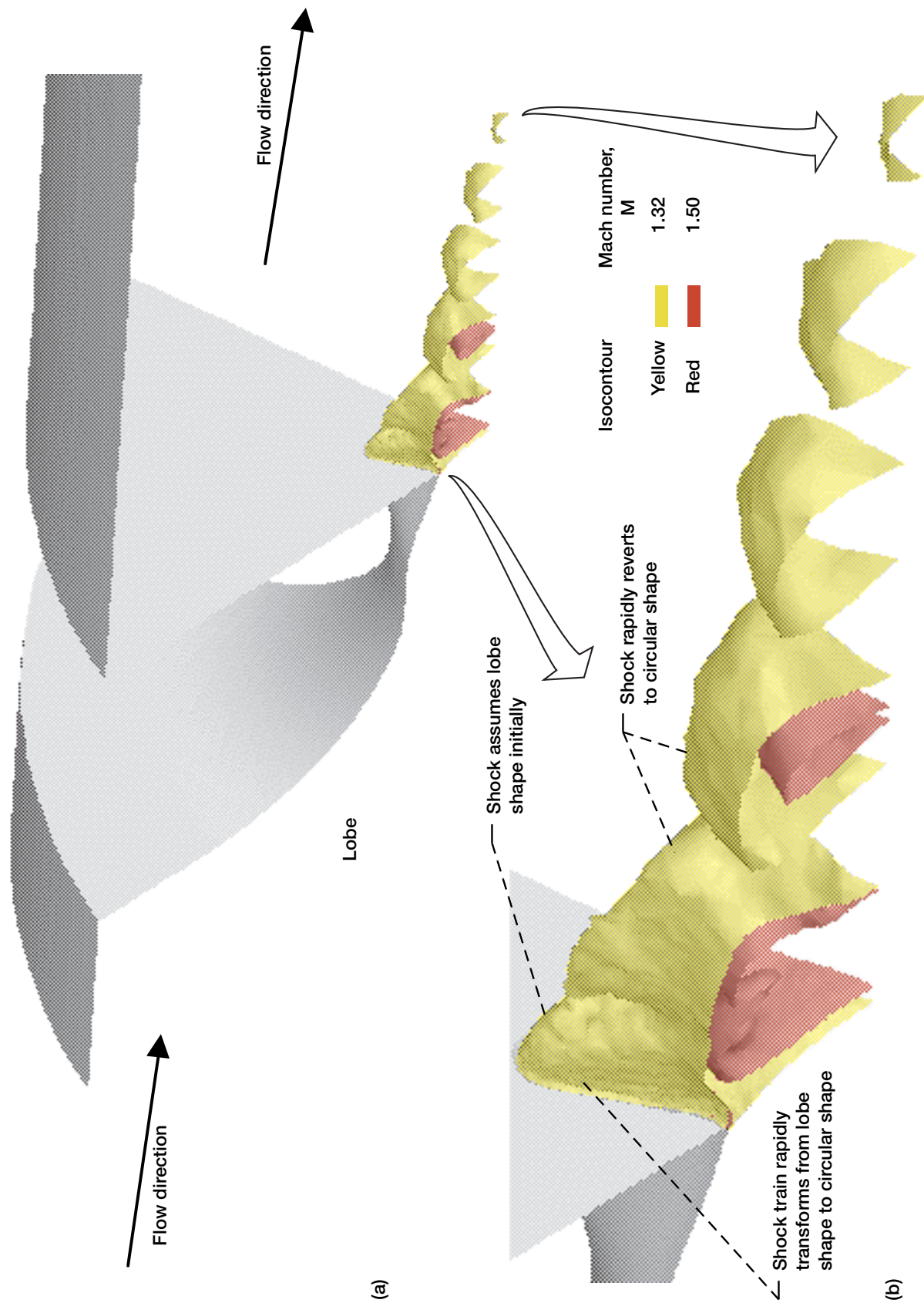
Figure 12.—Local shock pattern associated with lobed diffuser-mixer configuration, including shape transition and shock train dissipation. (a) Overall view. (b) Local details.

Flow direction

Isocontours | Mach number, M
Cyan | 0.94
Green | 1.12
Yellow | 1.32
Red | 1.50

Flow direction

Supersonic jet core flow with shock train

Fully supersonic core flow with discrete structures

Sonic surface between cyan and green contours

(a)

(b)
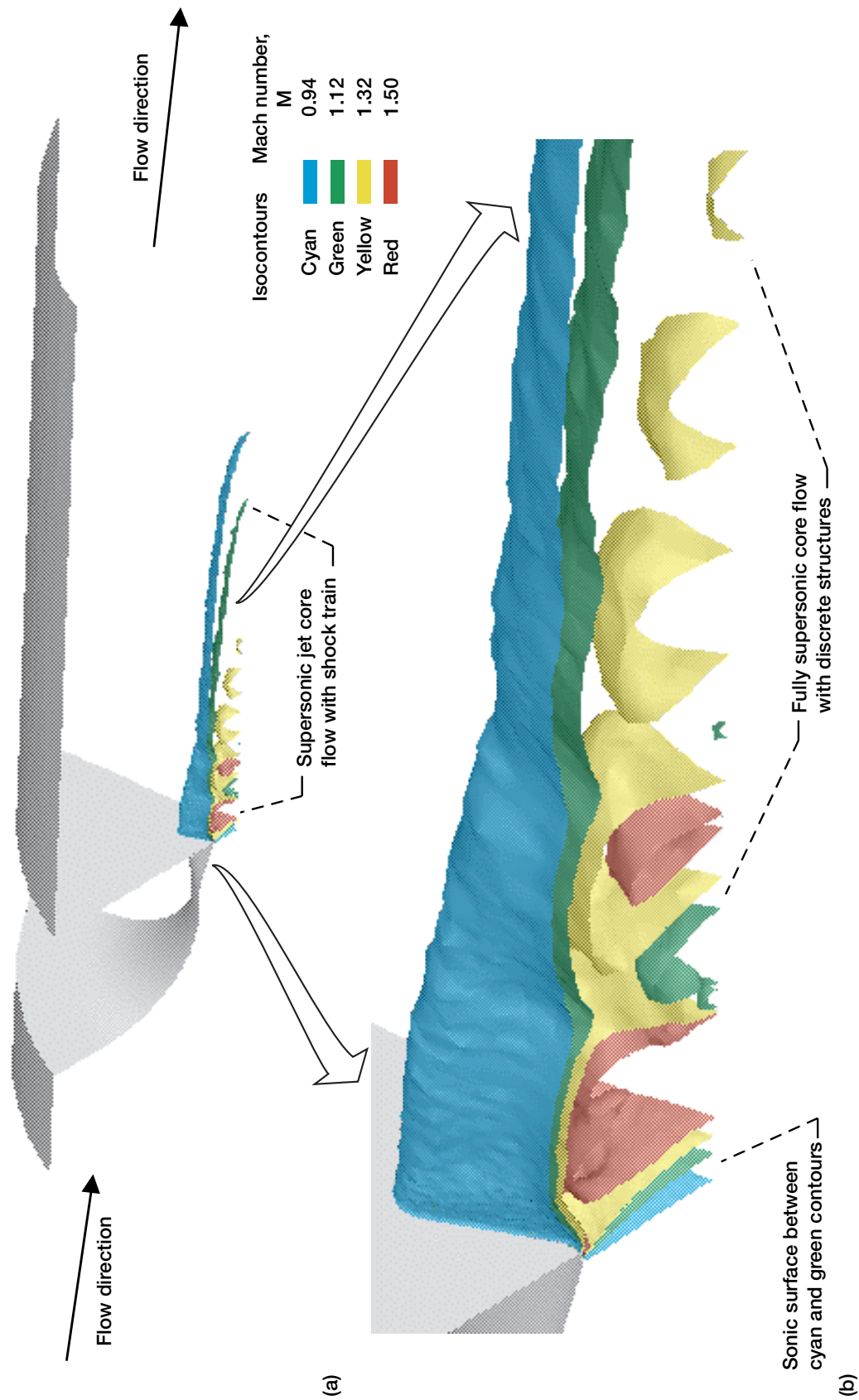
Figure 13.—Cellular shock structure in near field of lobe exit. (a) Overall view. (b) Local details.
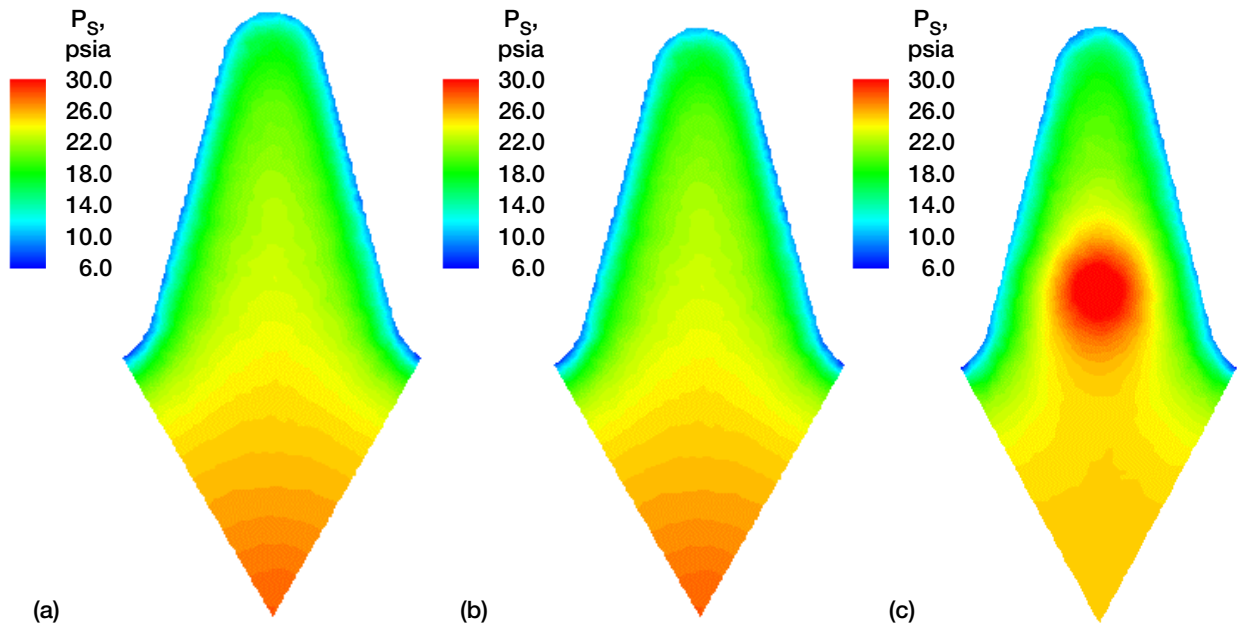
Figure 14.—Distortion of static pressure P_S field due to pitot probe, shown at lobe exit plane Z = 0.00 in. (flush with tip of pitot probe). (a) Baseline CFD solution without probe. (b) CFD solution with probe along centerline. (c) CFD solution with probe offset at radius of 0.75 in. in lobe valley.
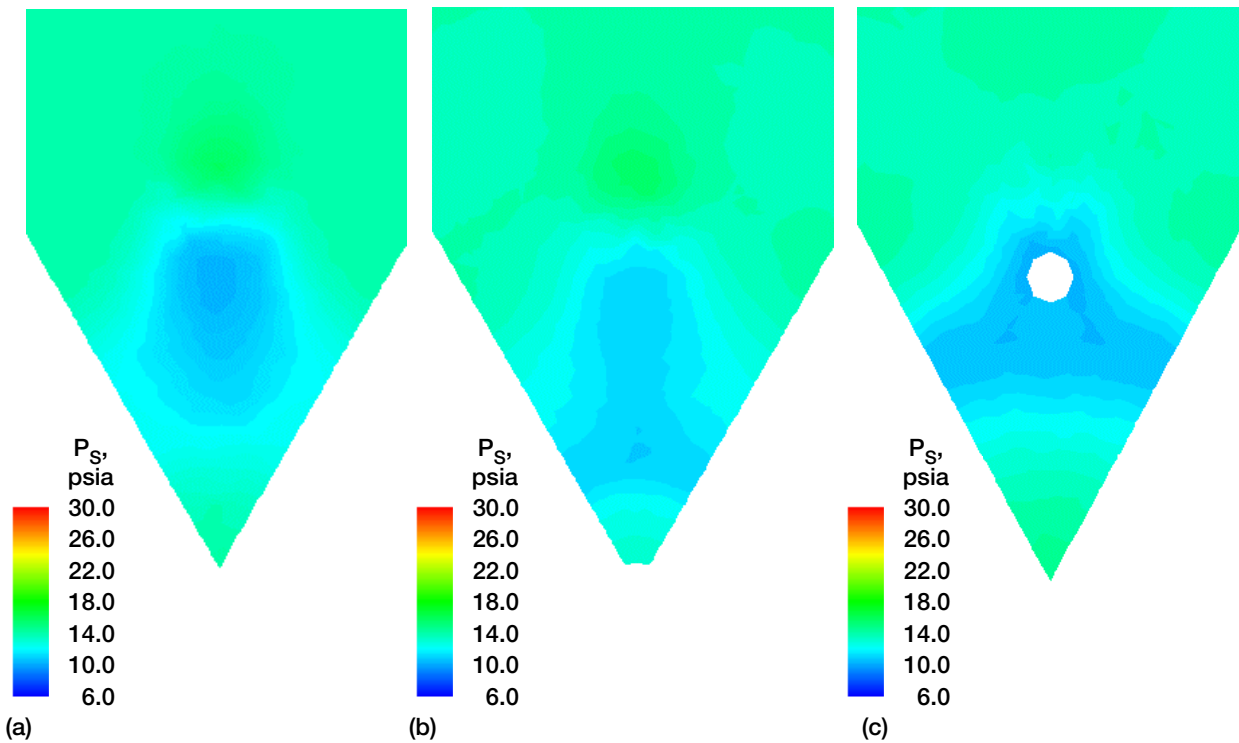
Figure 15.—Distortion of static pressure P_S field due to pitot probe, shown at 0.50 in. downstream of lobe exit plane. All contours taken at 0.50 in. downstream of lobe exit plane, coincident with location of static pressure ports on probe. (a) Baseline CFD solution without probe. (b) CFD solution with probe aligned along centerline. (c) CFD solution with probe in lobe valley, offset at radius of 0.75 in.
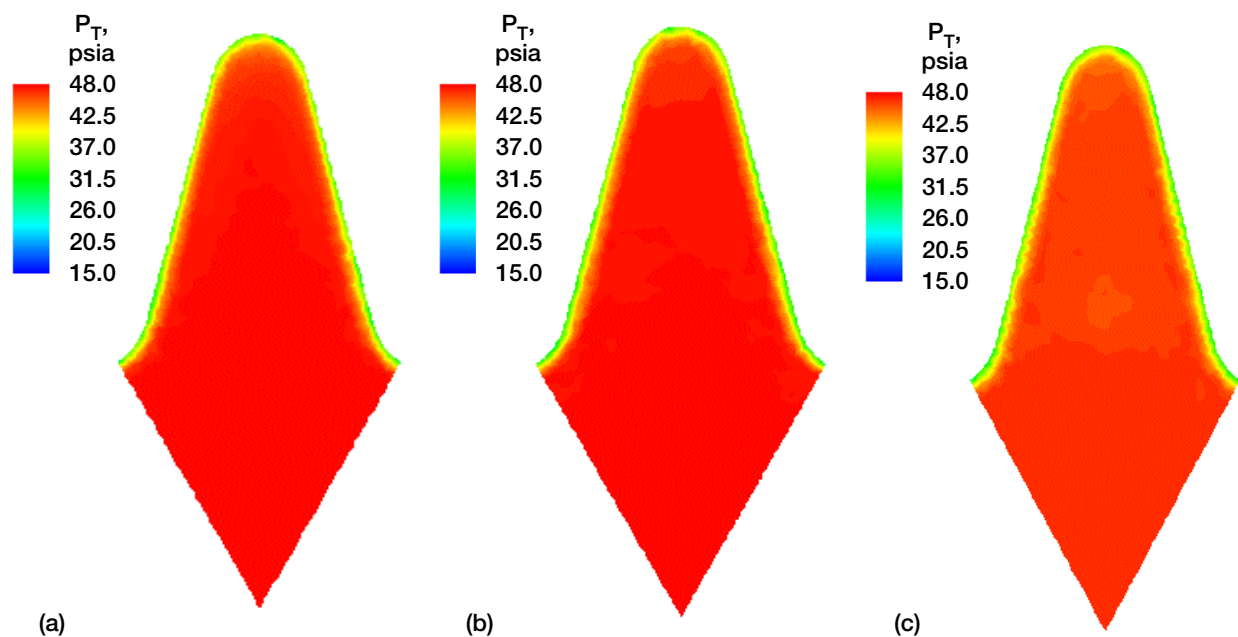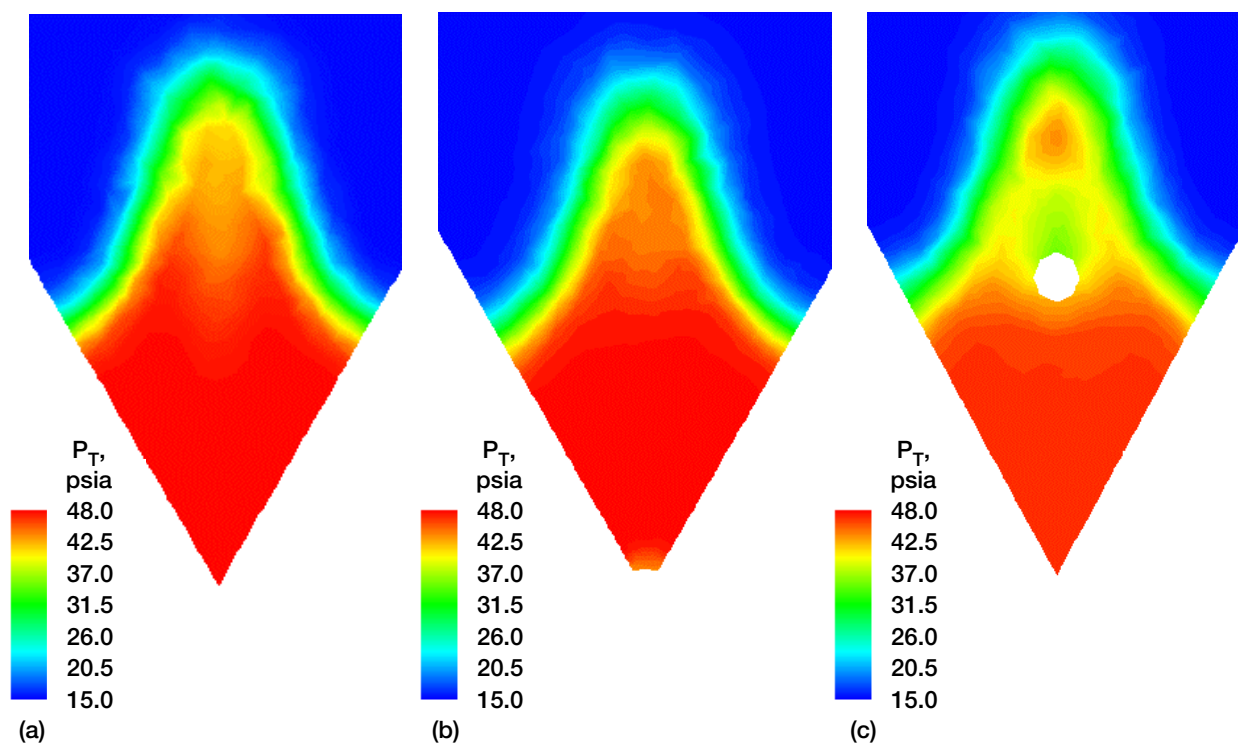
Figure 16.—Total pressure P_T contours with and without pitot probe, shown at lobe exit plane Z = 0.00 in. (flush with tip of pitot probe). No total pressure flow-field distortions observed at this plane. (a) Baseline CFD solution without probe. (b) CFD solution with probe aligned along centerline. (c) CFD solution with probe in lobe valley.

Figure 17.—Total pressure P_T contours with and without pitot probe, shown in plane of static pressure ports 0.50 in. downstream of lobe exit plane, coincident with the location of static pressure ports on probe. (a) Baseline CFD solution without probe. (b) CFD solution with probe aligned along centerline. (c) CFD solution with probe in lobe valley, offset at radius of 0.75 in.
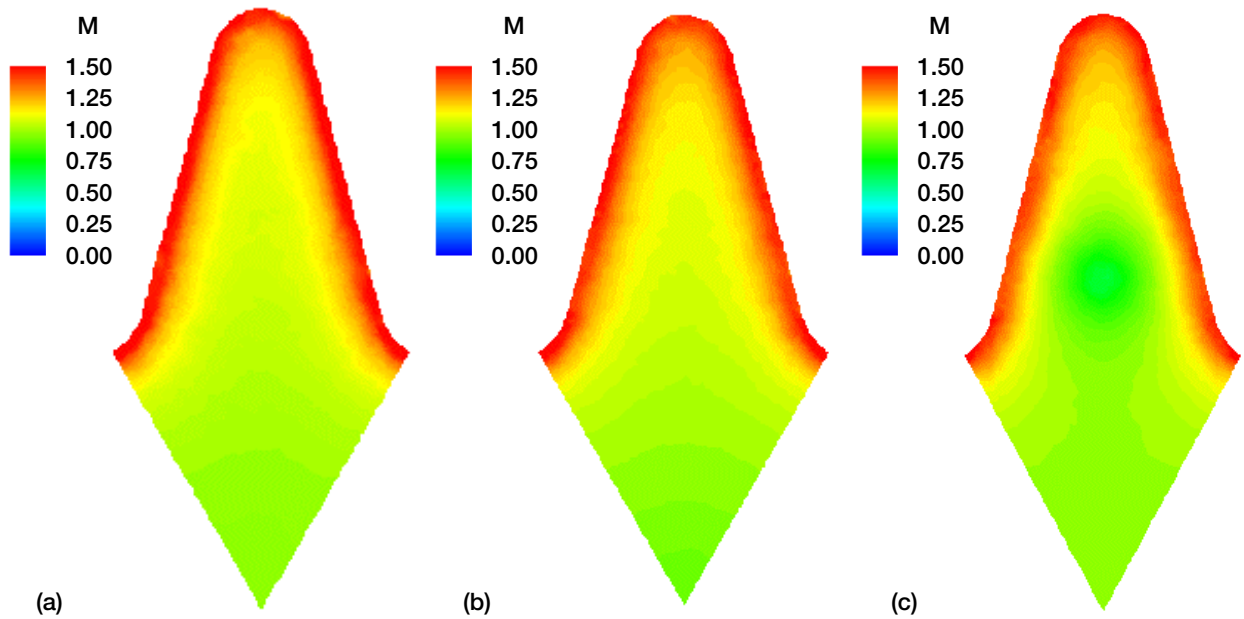
Figure 18.—Mach number M contours with and without pitot probe, shown in lobe exit plane Z = 0.00 in. (flush with tip of pitot probe). (a) Baseline CFD solution without probe. (b) CFD solution with probe aligned along centerline. (c) CFD solution with probe in lobe valley, offset at radius of 0.75 in.
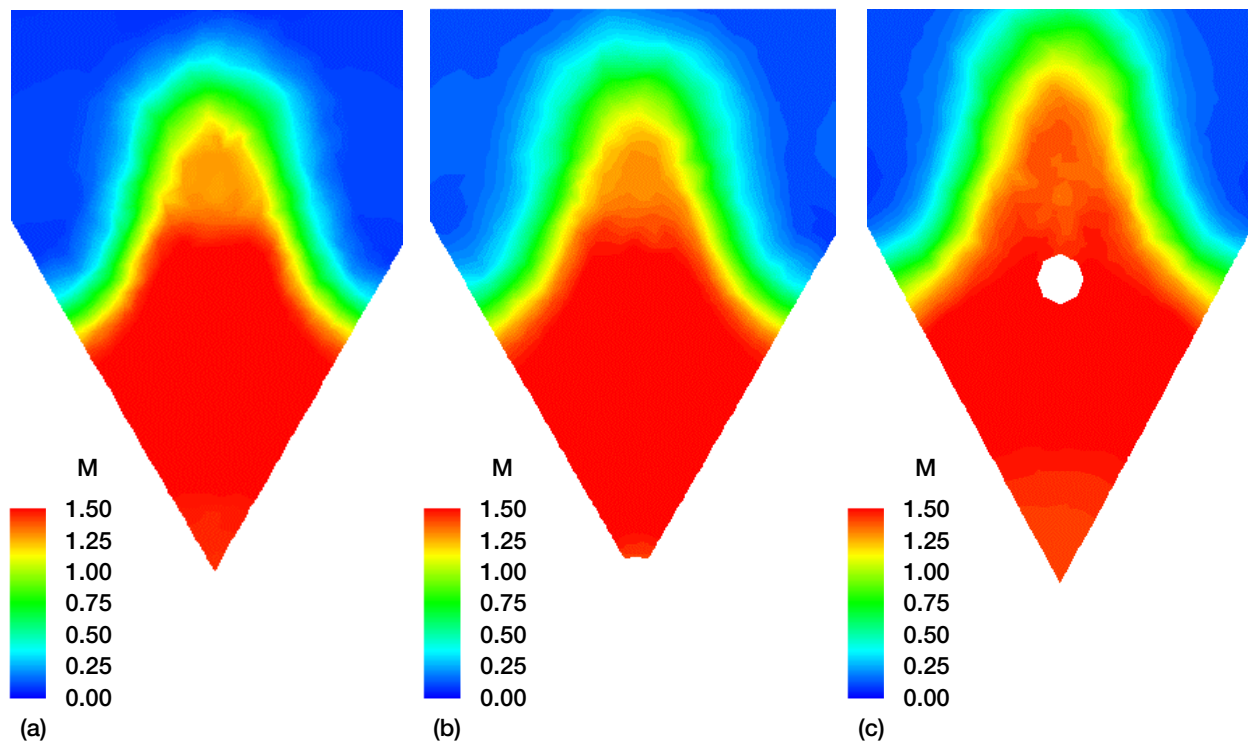

Figure 19.—Mach number M contours with and without pitot probe, shown in 0.50 in. downstream of lobe exit plane, coincident with location of static pressure ports on probe at four-hole static location on pitot probe. (a) Baseline CFD solution without probe. (b) CFD solution with probe aligned along centerline. (c) CFD solution with probe in lobe valley, offset at radius of 0.75 in.
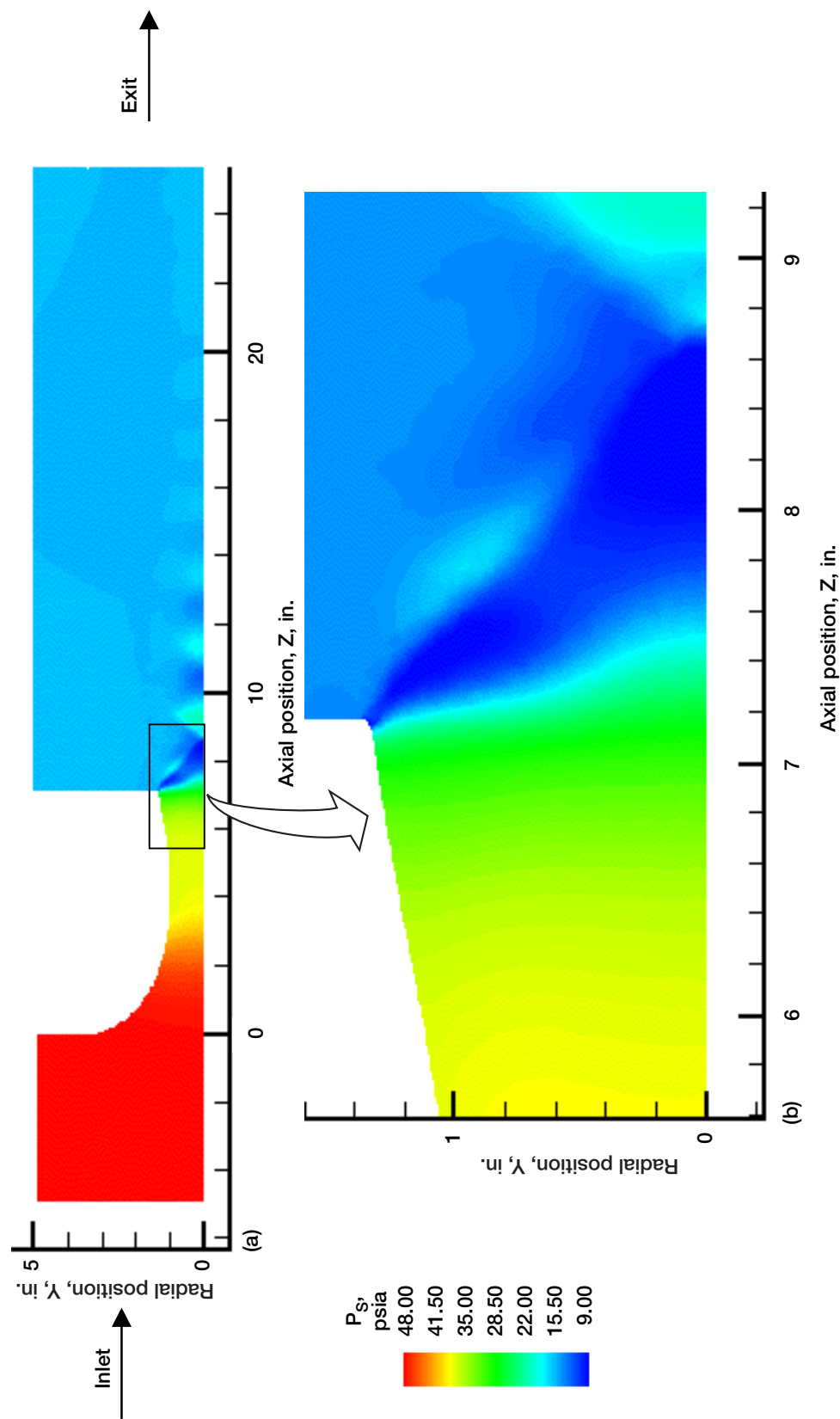
Figure 20.—Axial variation in static pressure P_S along lobed diffuser-mixer valley, without pitot probe. (a) Overall view, showing multiple cellular shock structures. (b) Detail in vicinity of exit plane.
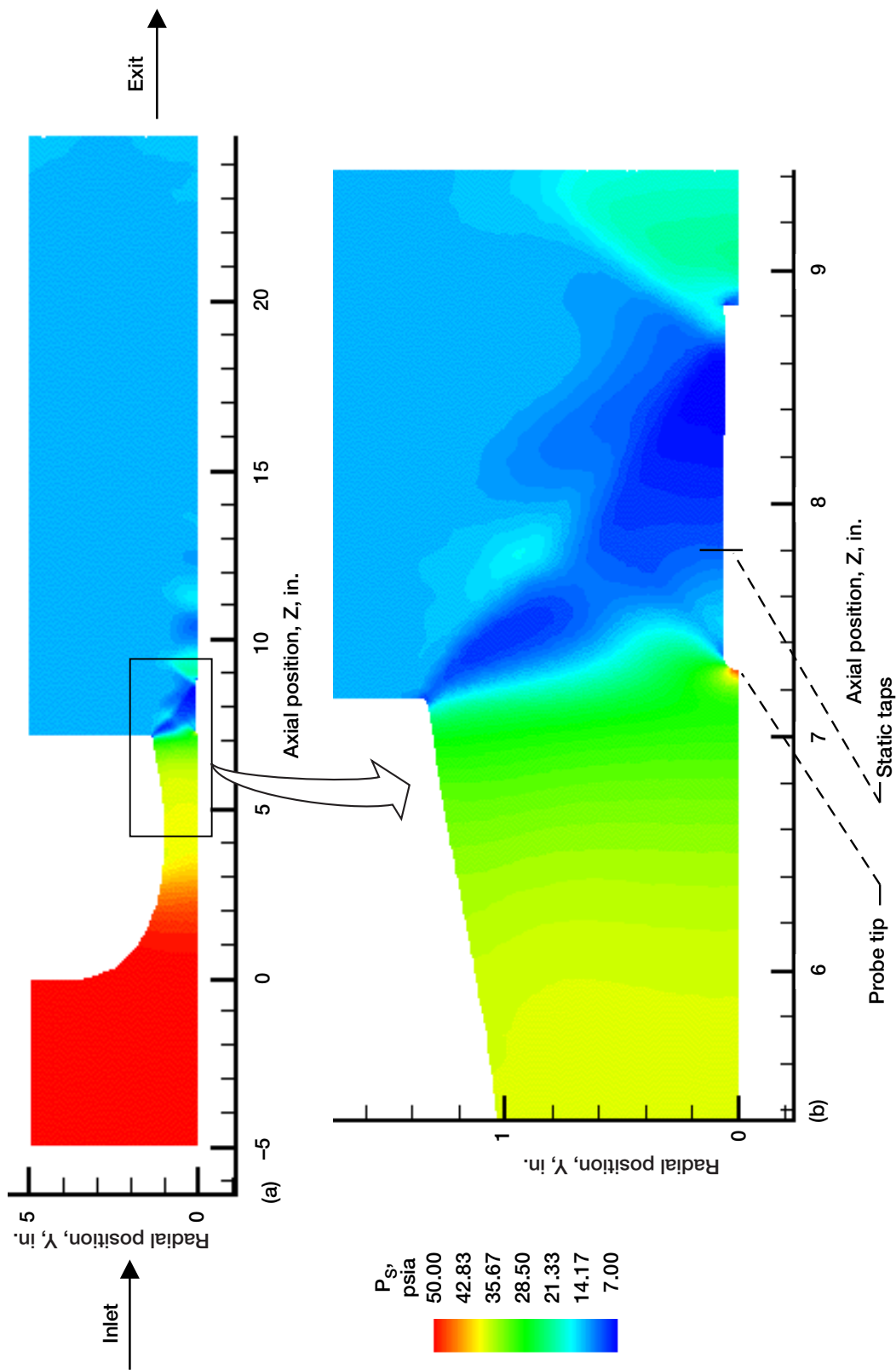
Figure 21.—Axial variation in static pressure P_S along lobed diffuser-mixer valley with pitot probe (0.125-in. diameter; head, 1.5 in. long) along duct centerline. Static taps located 0.50 in. behind tip of probe. (a) Overall view, showing shock interaction with probe. (b) Detail of pressure variation along probe tube.
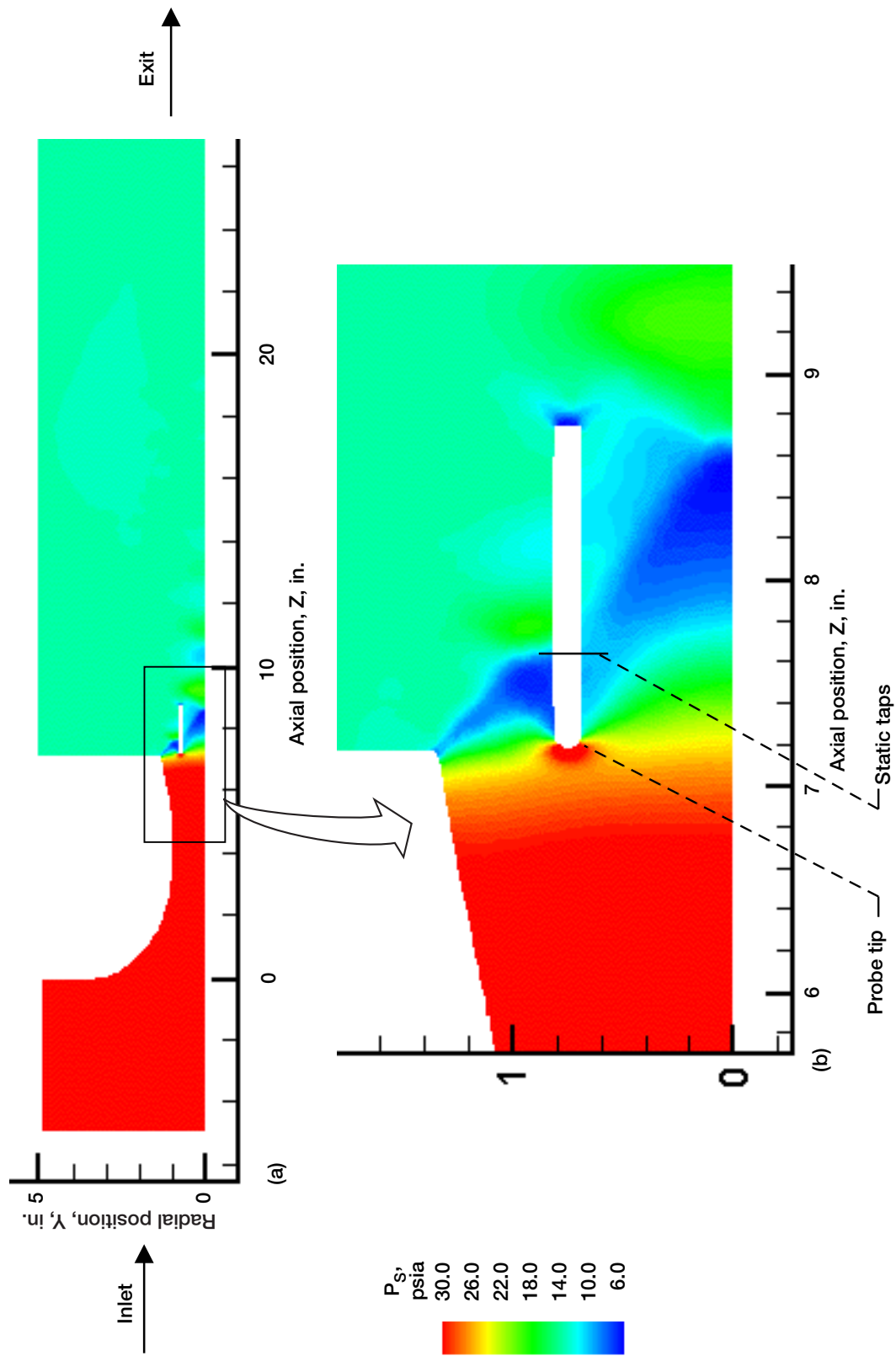
Figure 22.—Axial variation in static pressure P_S along lobed diffuser-mixer valley with pitot probe (0.125-in. diameter; head, 1.50 in. long) along duct centerline. Static taps located 0.50 in. behind tip of probe. (a) Overall view, showing shock interaction with probe. (b) Detail of pressure variation along probe tube.
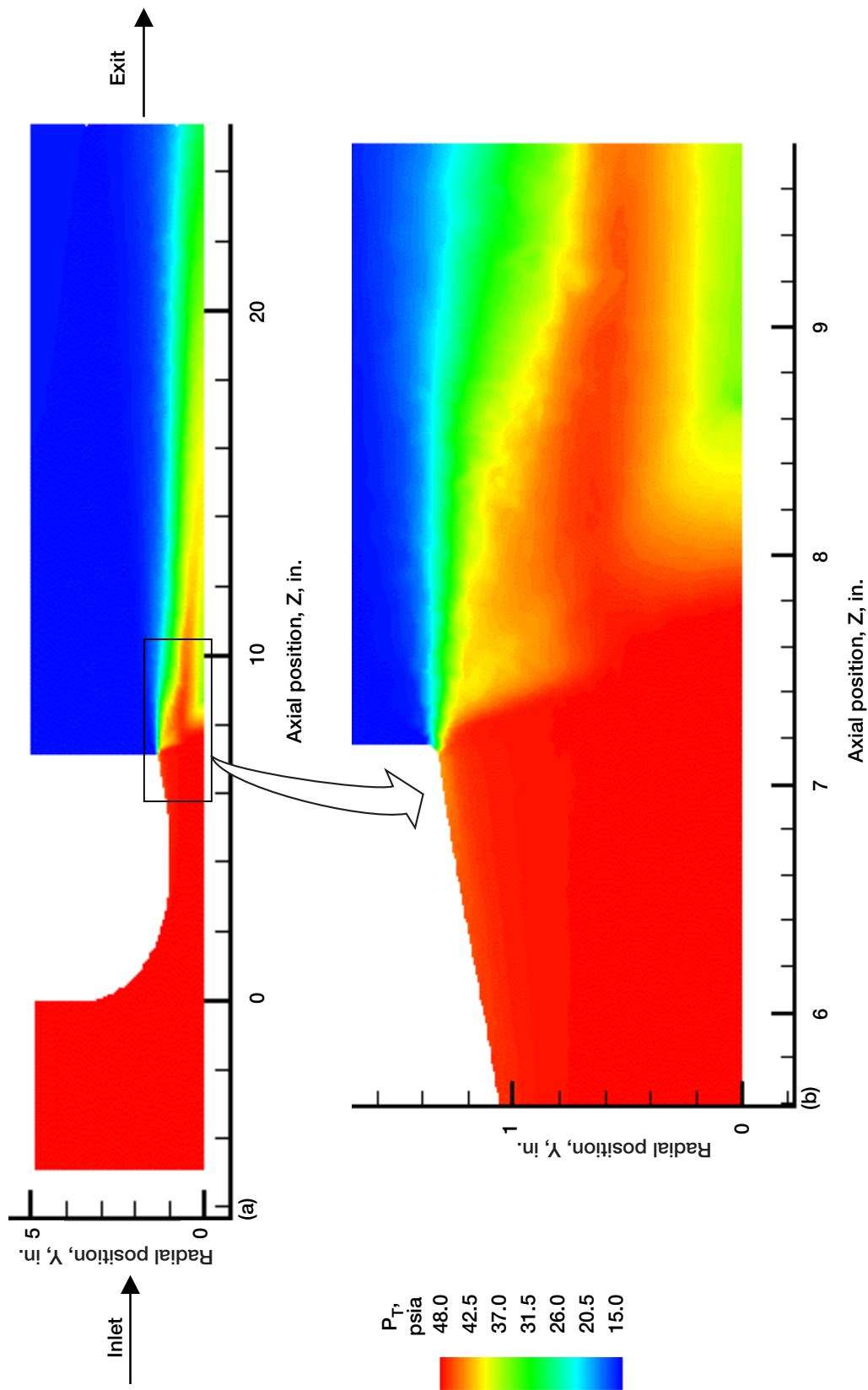
Figure 23.—Axial variation in total pressure P_T along lobed diffuser-mixer valley without pitot probe. (a) Overall view showing axial variation of pressure losses as jet issues into large pipe. (b) Detail in vicinity of exit plane.
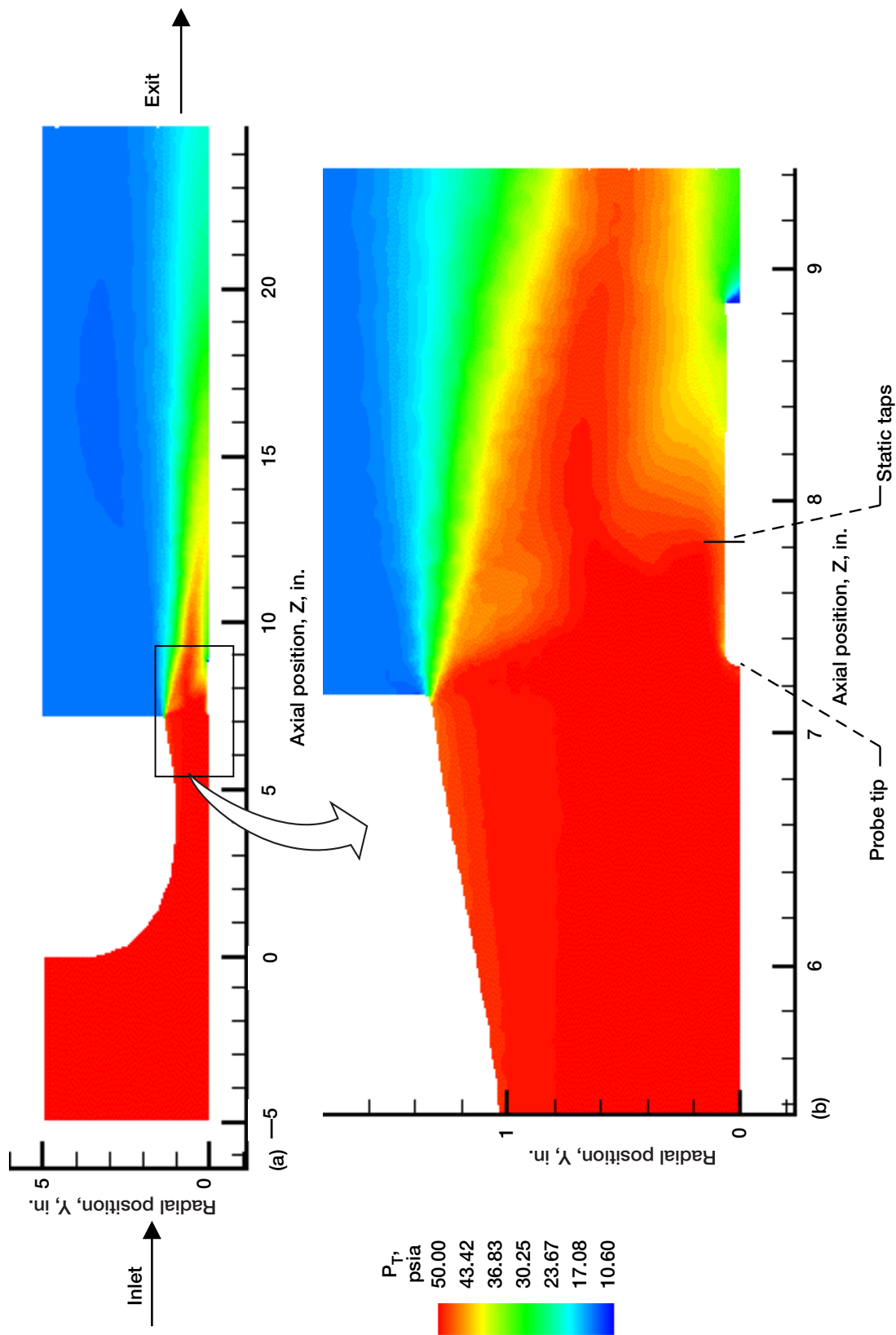
Figure 24.—Axial variation in total pressure P_T along lobed diffuser-mixer valley with pitot probe (0.125-in. diameter; head, 1.5 in. long) along duct centerline. Static taps located 0.50 in. behind tip of probe. (a) Overall view of pressure losses as jet issues into large pipe. (b) Detail along probe surface, near exit plane.
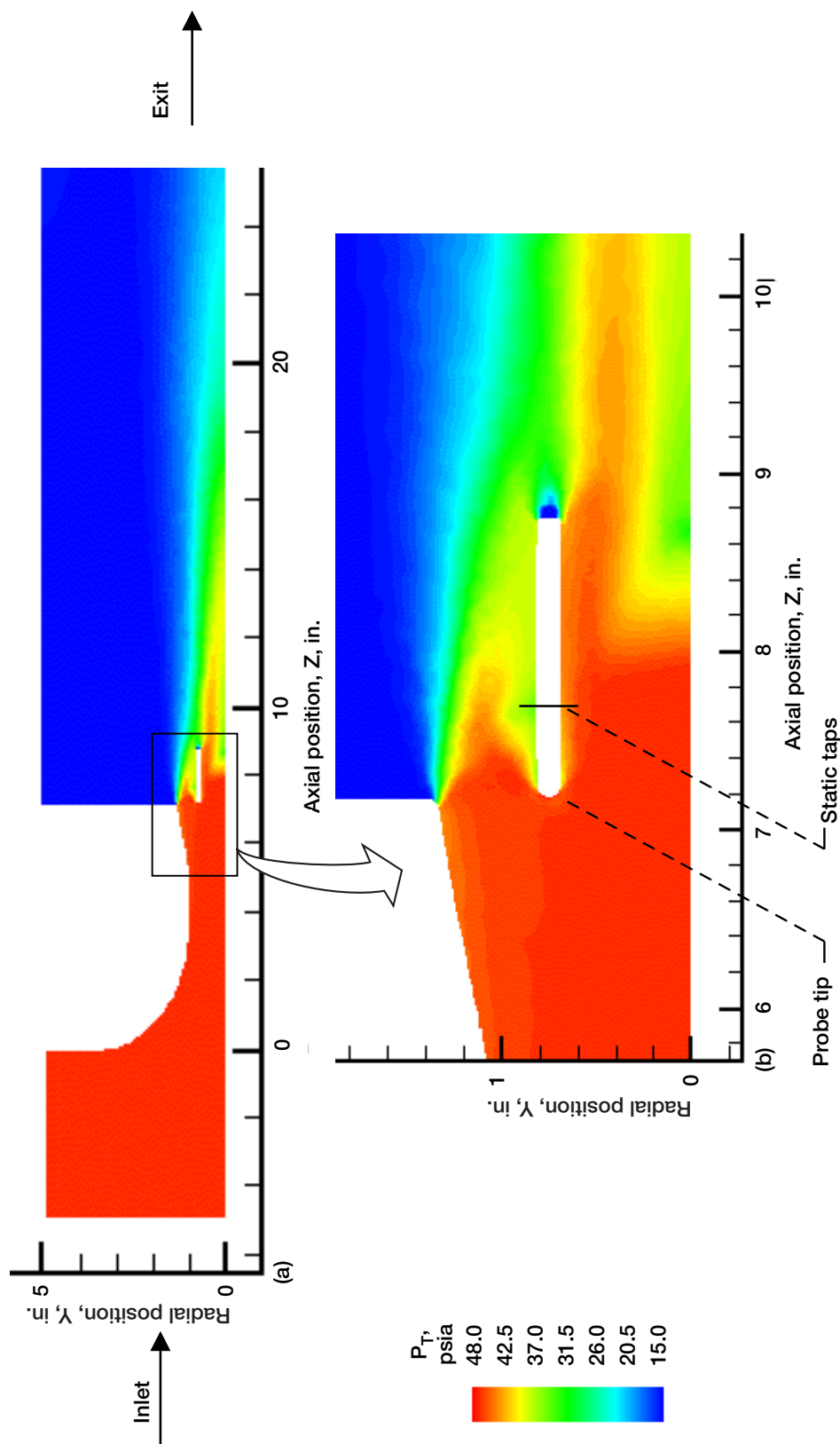
Figure 25.—Axial variation in total pressure P_T along lobed diffuser-mixer valley with pitot probe (0.125-in.diameter; head, 1.5 in. long) offset at radius of 0.75 in. Static taps located 0.50 in. behind tip of probe. (a) Overall view of distortion in pressure losses as jet issues into large pipe. (b) Detail along probe surface, near exit plane.
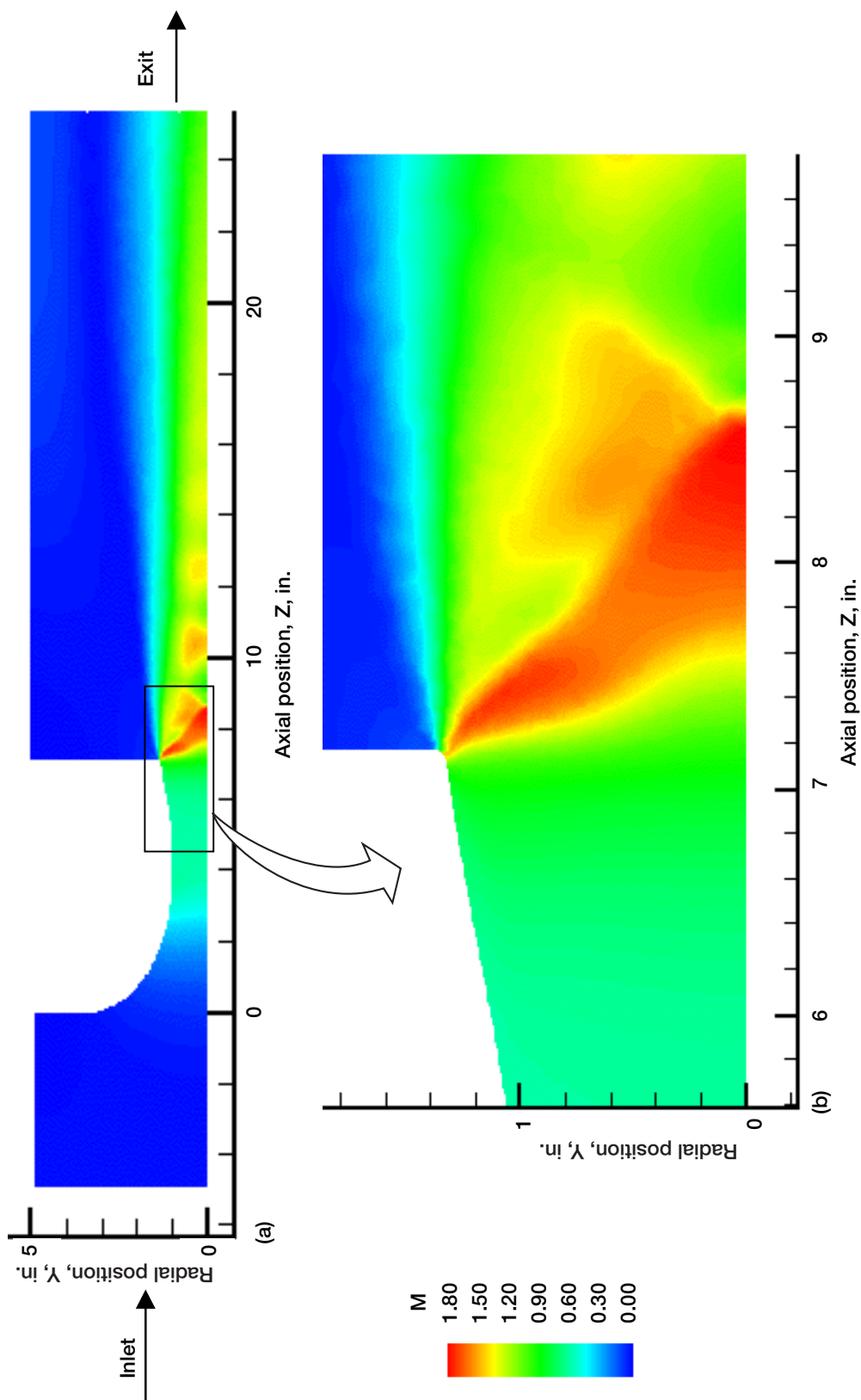
Figure 26.—Axial variation in mach number M along lobed diffuser-mixer valley without pitot probe. (a) Overall view showing axial dissipation of shocks as jet issues into large pipe. (b) Detail in vicinity of exit plane.
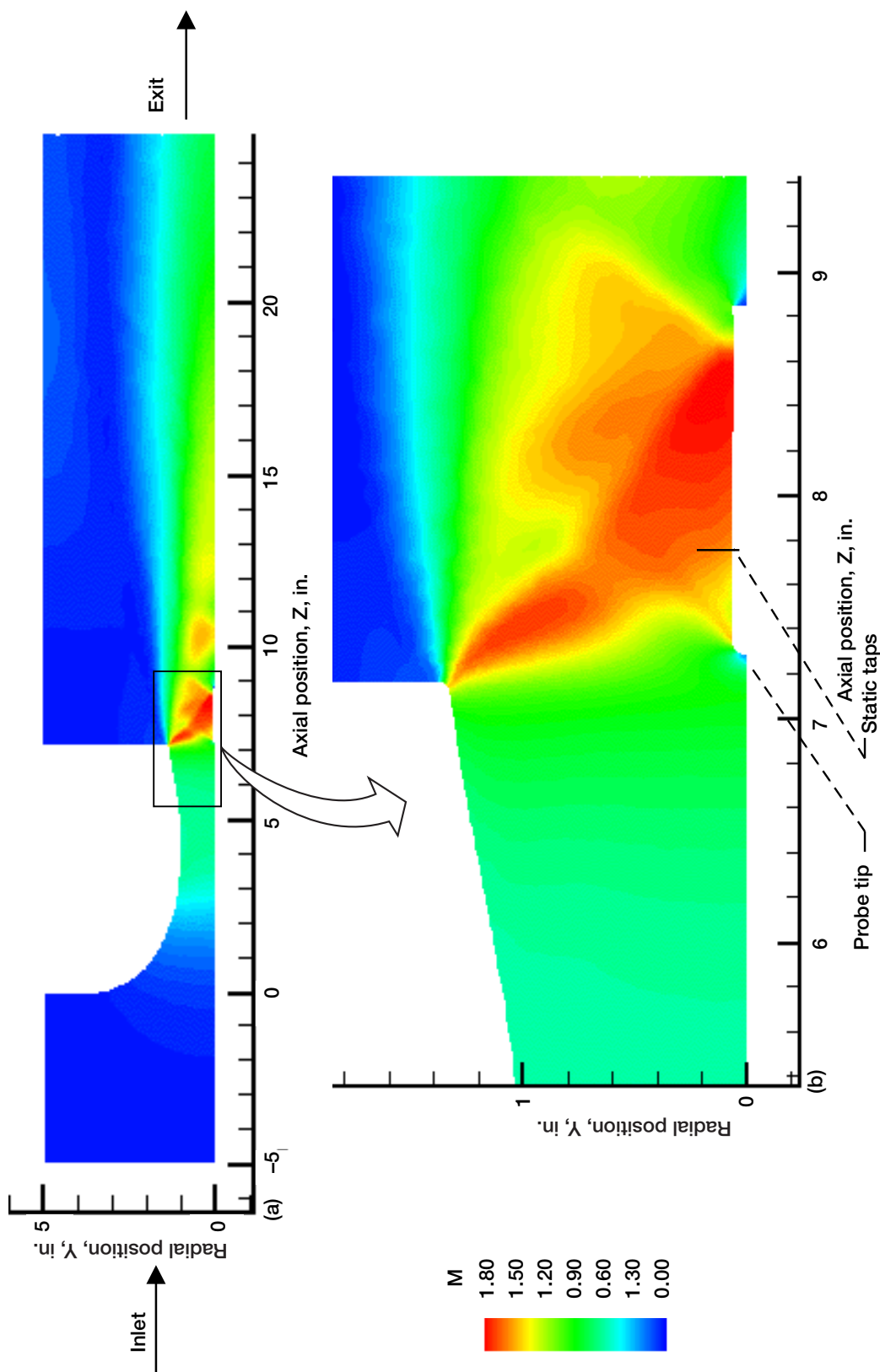
Figure 27.—Axial variation in mach number M along the lobed diffuser-mixer valley with pitot probe (0.125-in. diameter; head, 1.5 in. long) along duct centerline. Static taps located 0.50 in. behind tip of probe. (a) Overall view of probe. (b) Detail of variation along probe surface near exit plane.
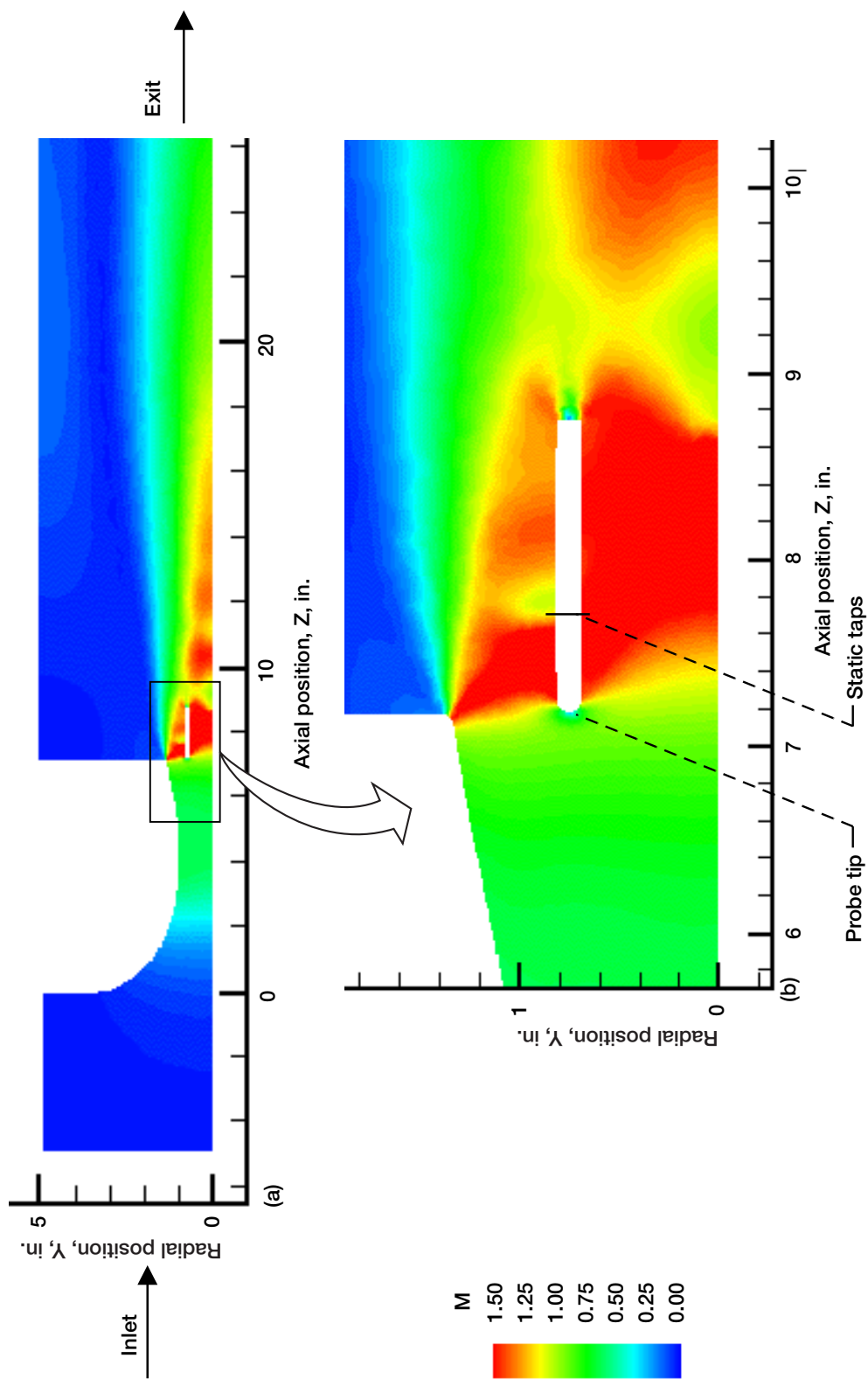
Figure 28.—Axial variation in mach number M along lobed diffuser-mixer valley with pitot probe (0.125-in. diameter; head, 1.5 in. long) offset at radius of 0.75 in. Static taps located 0.50 in. behind tip of probe. (a) Overall view of distortion of shock pattern as jet issues into large pipe. (b) Detail of variation along probe surface near exit plane.

Z = 7.65 in. (+0.50 in.)

Z = 7.40 in. (+0.25 in.)

Z = 7.15 in.
(0.0 in., exit plane)

Z = 6.90 in. (–0.25 in.)

Z = 8.65 in. (+1.50 in.)

Z = 8.40 in. (+1.25 in.)

Z = 8.15 in. (+1.00 in.)

Z = 7.90 in. (+0.75 in.)

P_S,
psia
30.0
26.0
22.0
18.0
14.0
10.0
6.0

Figure 29.—Axial slices of static pressure P_S contour through lobed diffuser-mixer from 0.25 in. upstream to 1.50 in. downstream of exit plane.
Without pitot probe.

P_T, psia

48.0
42.5
37.0
31.5
26.0
20.5
15.0

Z = 6.90 in. (−0.25 in.)

Z = 7.15 in.
(0.0 in., exit plane)

Z = 7.40 in. (+0.25 in.)

Z = 7.65 in. (+0.50 in.)

Z = 7.90 in. (+0.75 in.)

Z = 8.15 in. (+1.00 in.)

Z = 8.40 in. (+1.25 in.)
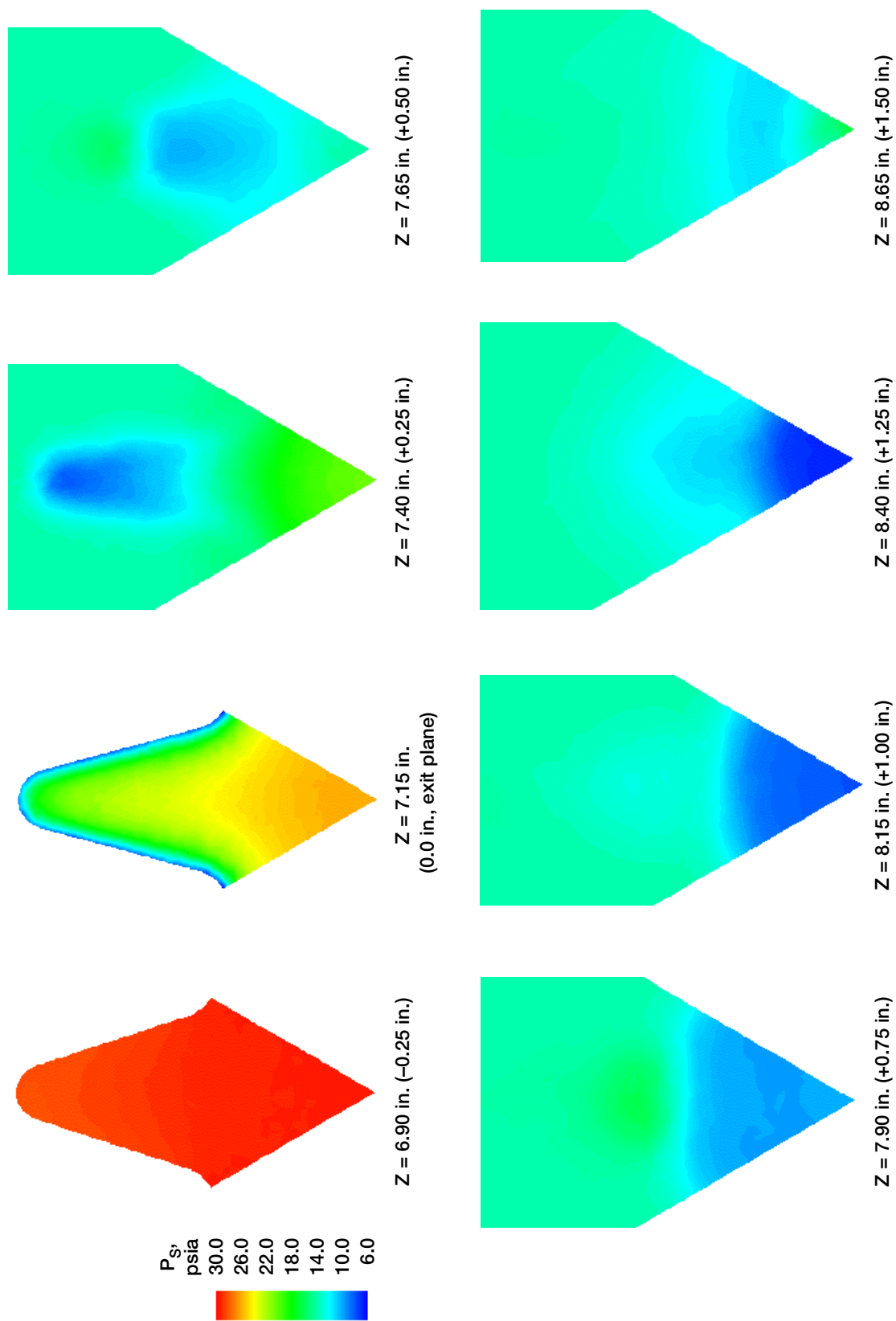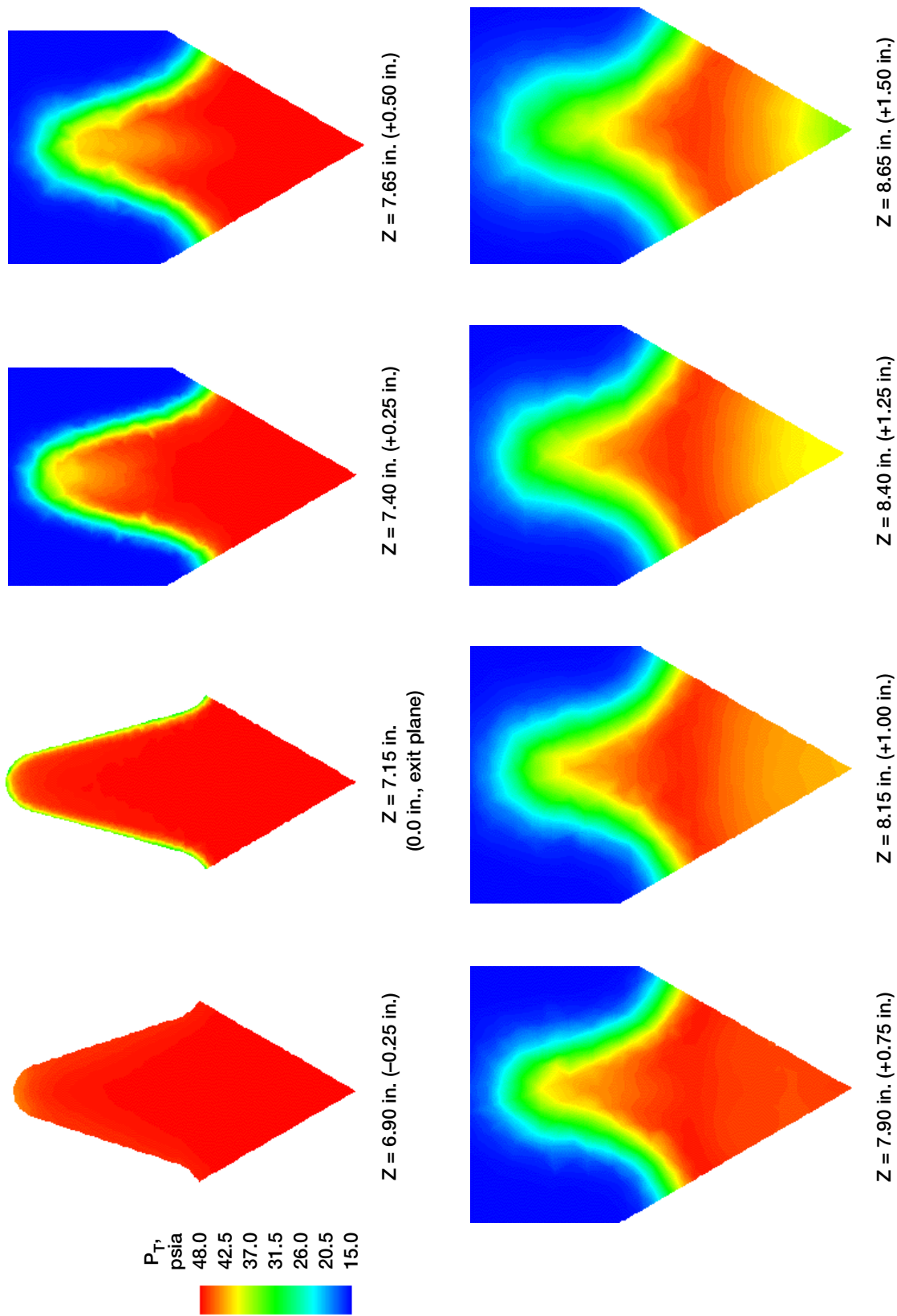
Z = 8.65 in. (+1.50 in.)

Figure 30.—Axial slices of total pressure P_T contour through lobed diffuser-mixer from 0.25 in. upstream to 1.50 in. downstream of exit plane. Without pitot probe.

M
1.50
1.25
1.00
0.75
0.50
0.25
0.00

Z = 6.90 in. (−0.25 in.)

Z = 7.15 in.
(0.0 in., exit plane)

Z = 7.40 in. (+0.25 in.)

Z = 7.65 in. (+0.50 in.)

Z = 7.90 in. (+0.75 in.)

Z = 8.15 in. (+1.00 in.)
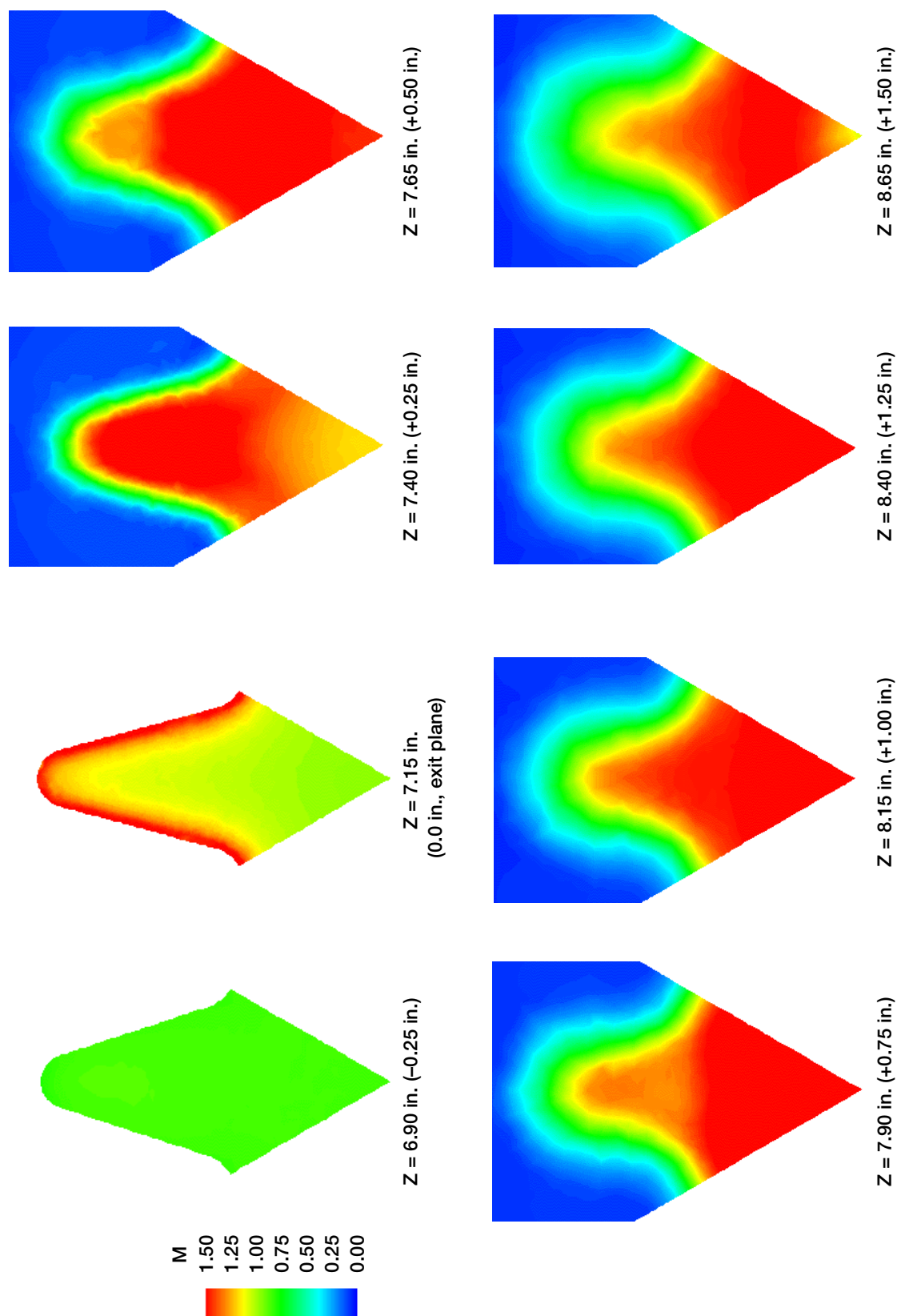
Z = 8.40 in. (+1.25 in.)

Z = 8.65 in. (+1.50 in.)

Figure 31.—Axial slices of mach number M contour through lobed diffuser-mixer from 0.25 in. upstream to 1.50 in. downstream of exit plane. Without pitot probe.
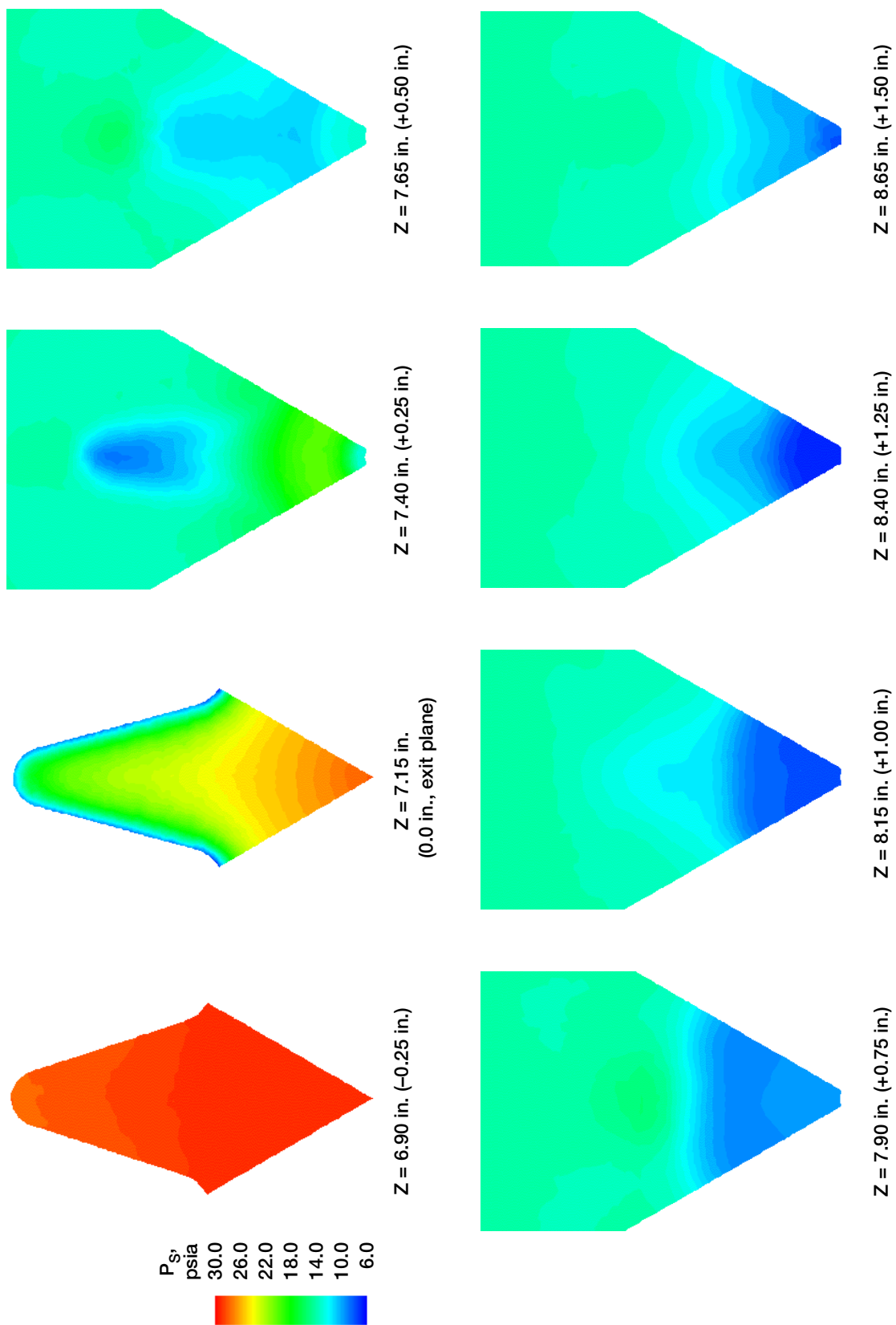
Figure 32.—Axial slices of static pressure P_S contour through lobed diffuser-mixer from 0.25 in. upstream to 1.50 in. downstream of exit plane. With pitot probe along duct centerline.

P_T, psia
48.0
42.5
37.0
31.5
26.0
20.5
15.0

Z = 6.90 in. (–0.25 in.)

Z = 7.15 in.
(0.0 in., exit plane)

Z = 7.40 in. (+0.25 in.)

Z = 7.65 in. (+0.50 in.)

Z = 7.90 in. (+0.75 in.)

Z = 8.15 in. (+1.00 in.)

Z = 8.40 in. (+1.25 in.)
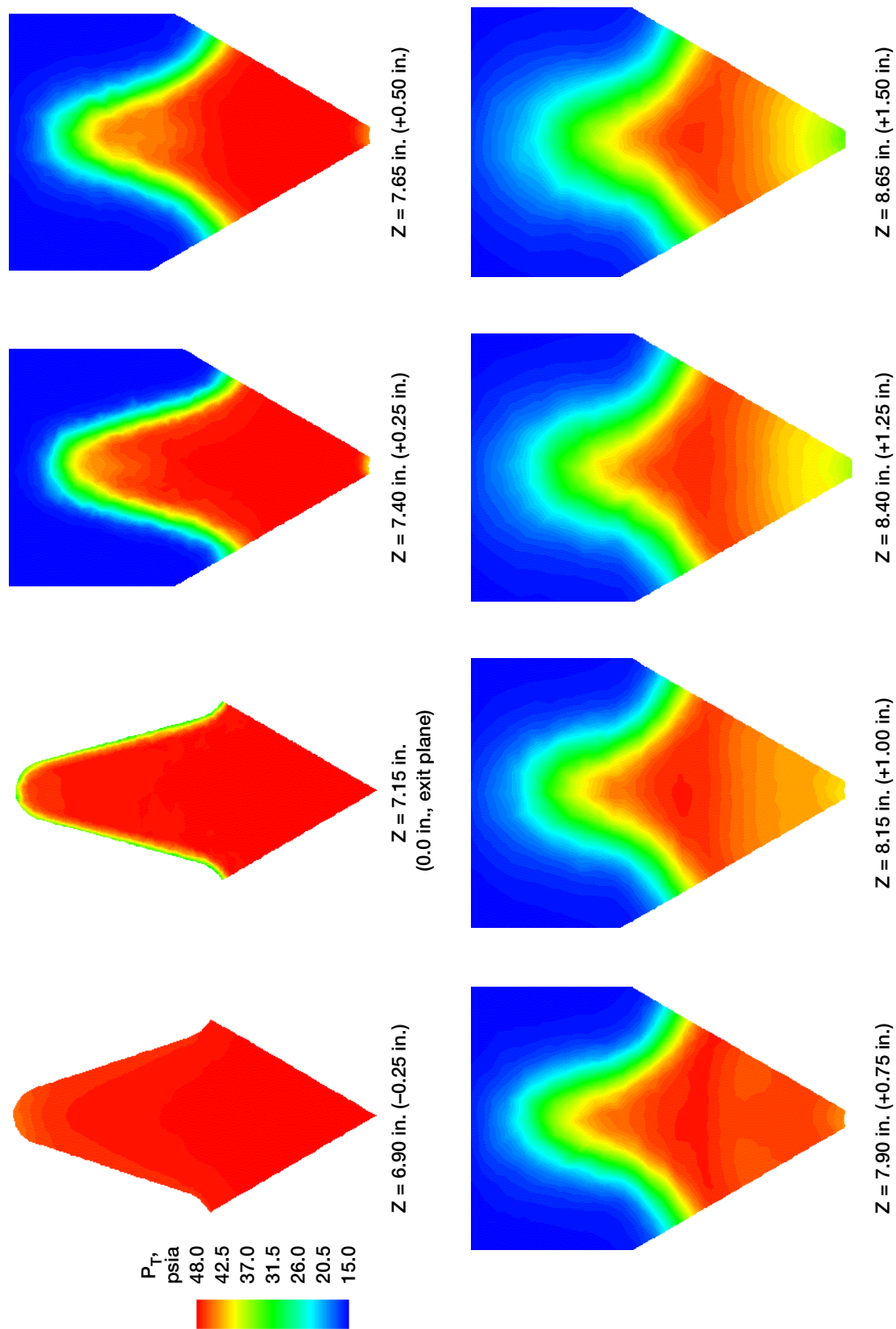
Z = 8.65 in. (+1.50 in.)

Figure 33.—Axial slices of total pressure P_T contour through lobed diffuser-mixer from 0.25 in. upstream to 1.50 in. downstream of exit plane. With pitot probe along duct centerline.

M
1.50
1.25
1.00
0.75
0.50
0.25
0.00

Z = 6.90 in. (−0.25 in.)

Z = 7.15 in.
(0.0 in., exit plane)

Z = 7.40 in. (+0.25 in.)

Z = 7.65 in. (+0.50 in.)

Z = 7.90 in. (+0.75 in.)

Z = 8.15 in. (+1.00 in.)
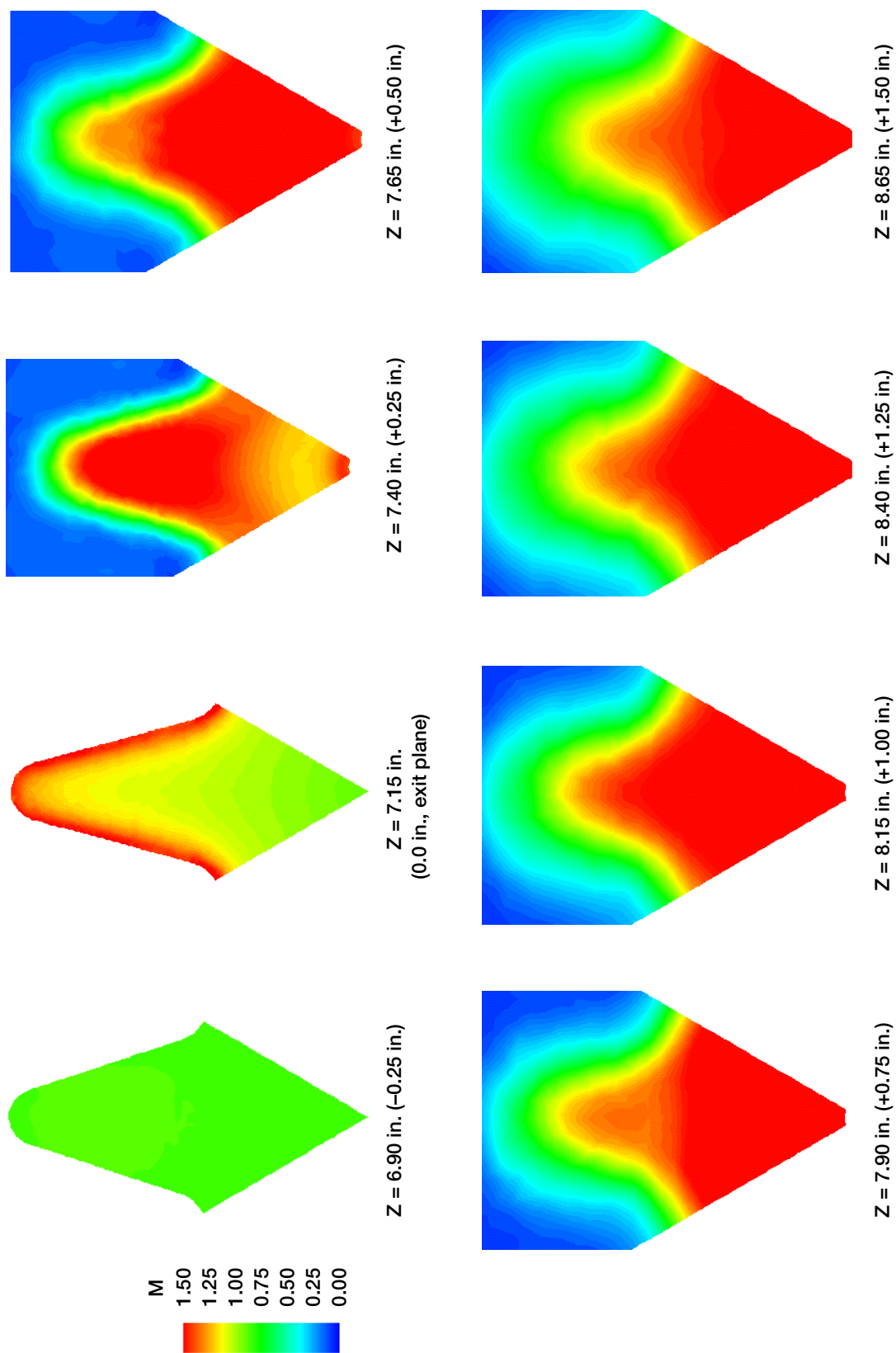
Z = 8.40 in. (+1.25 in.)

Z = 8.65 in. (+1.50 in.)

Figure 34.—Axial slices of mach number M contour through lobed diffuser-mixer from 0.25 in. upstream to 1.50 in. downstream of exit plane. With pitot probe along duct centerline.
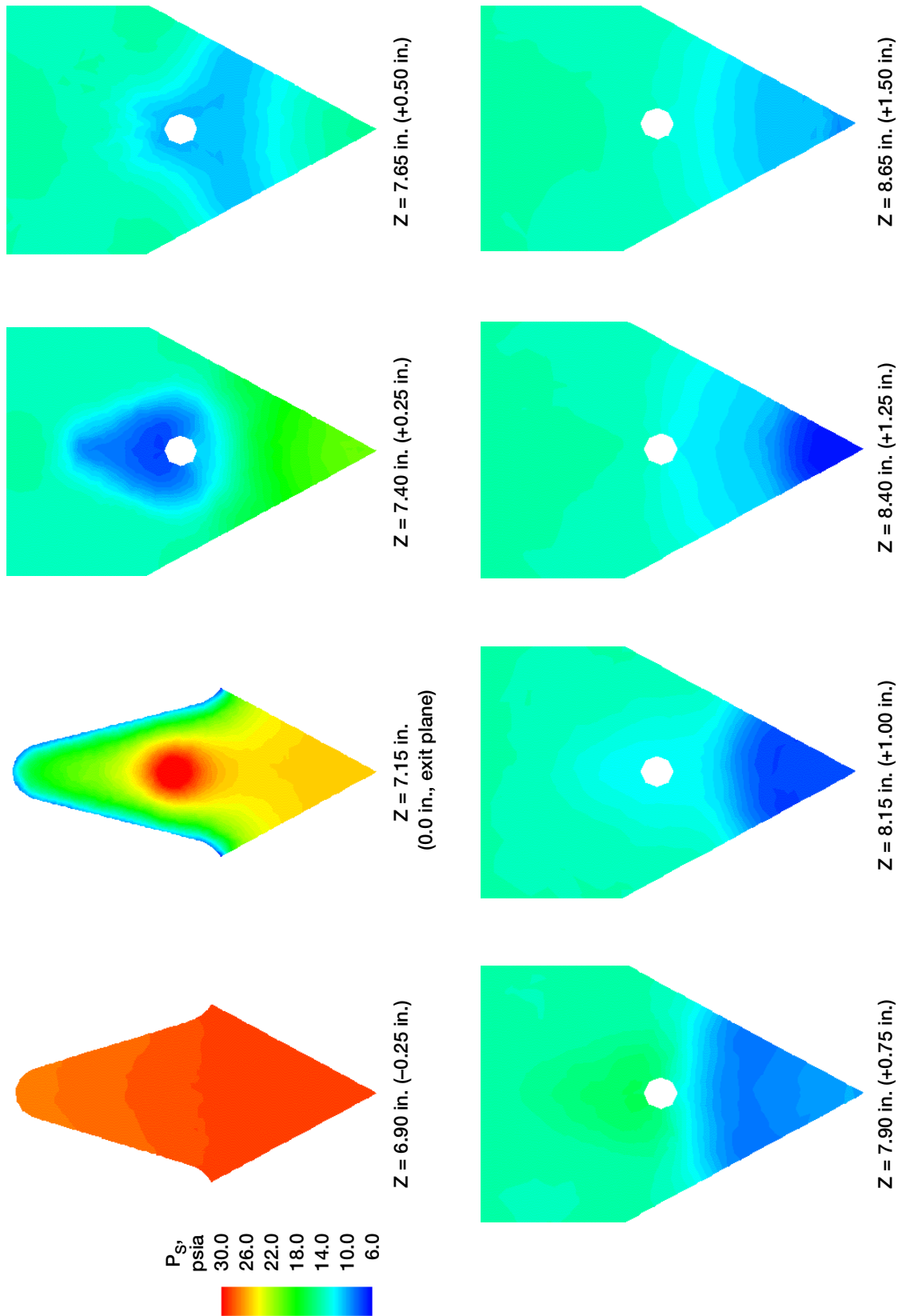
P_S, psia
30.0
26.0
22.0
18.0
14.0
10.0
6.0

Z = 6.90 in. (−0.25 in.)

Z = 7.15 in.
(0.0 in., exit plane)

Z = 7.40 in. (+0.25 in.)

Z = 7.65 in. (+0.50 in.)

Z = 7.90 in. (+0.75 in.)

Z = 8.15 in. (+1.00 in.)

Z = 8.40 in. (+1.25 in.)

Z = 8.65 in. (+1.50 in.)

Figure 35.—Axial slices of static pressure P_S contour through lobed diffuser-mixer from 0.25 in. upstream to 1.50 in. downstream of exit plane. With pitot probe offset 0.75 in. from duct centerline.
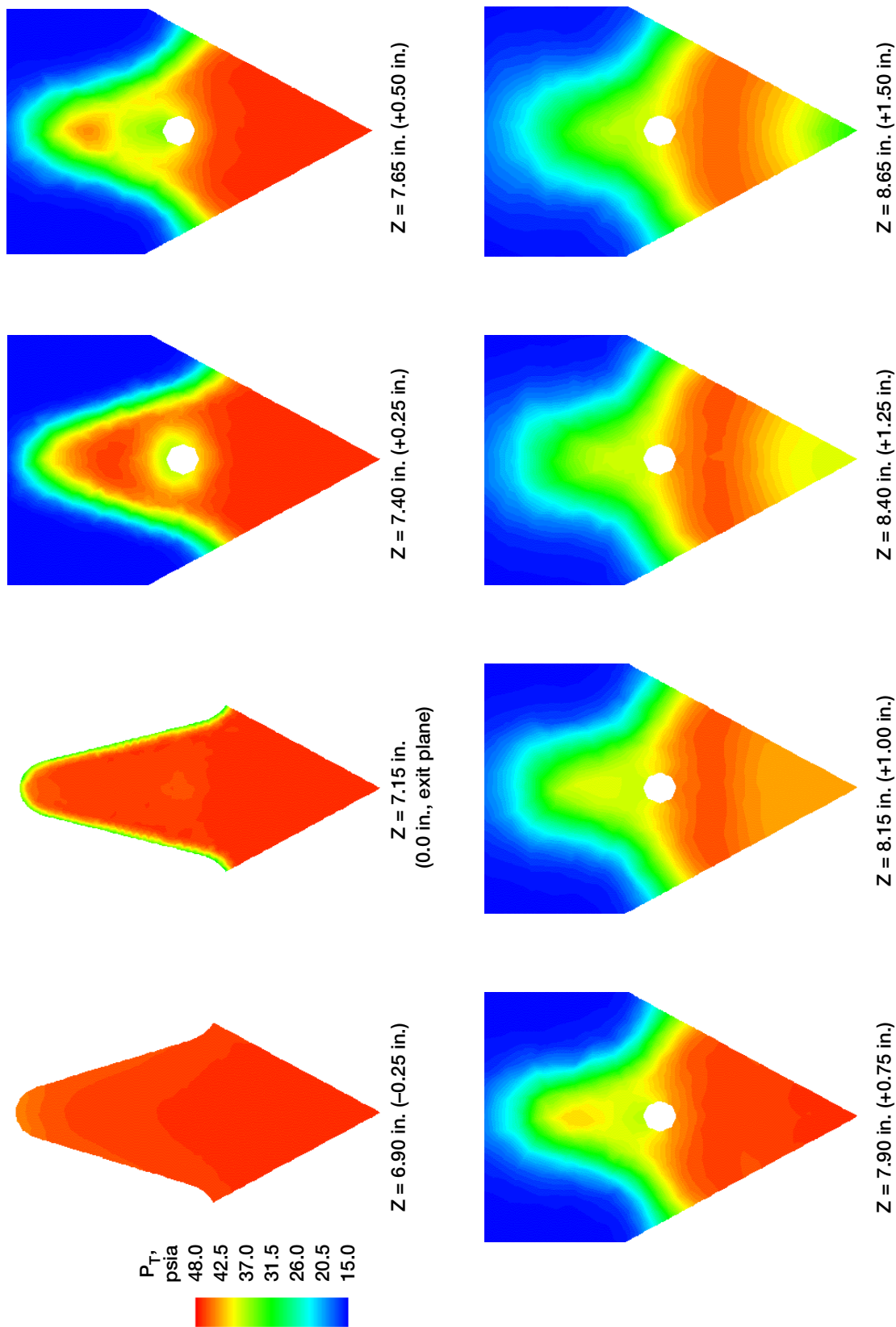
P_T, psia
48.0
42.5
37.0
31.5
26.0
20.5
15.0

Z = 7.65 in. (+0.50 in.)

Z = 7.40 in. (+0.25 in.)

Z = 7.15 in.
(0.0 in., exit plane)

Z = 6.90 in. (–0.25 in.)

Z = 8.65 in. (+1.50 in.)

Z = 8.40 in. (+1.25 in.)

Z = 8.15 in. (+1.00 in.)

Z = 7.90 in. (+0.75 in.)

Figure 36.—Axial slices of total pressure P_T contour through lobed diffuser-mixer from 0.25 in. upstream to 1.50 in. downstream of exit plane. With pitot probe offset 0.75 in. from duct centerline.

M
1.50
1.25
1.00
0.75
0.50
0.25
0.00

Z = 6.90 in. (−0.25 in.)

Z = 7.15 in.
(0.0 in., exit plane)

Z = 7.40 in. (+0.25 in.)

Z = 7.65 in. (+0.50 in.)

Z = 7.90 in. (+0.75 in.)

Z = 8.15 in. (+1.00 in.)

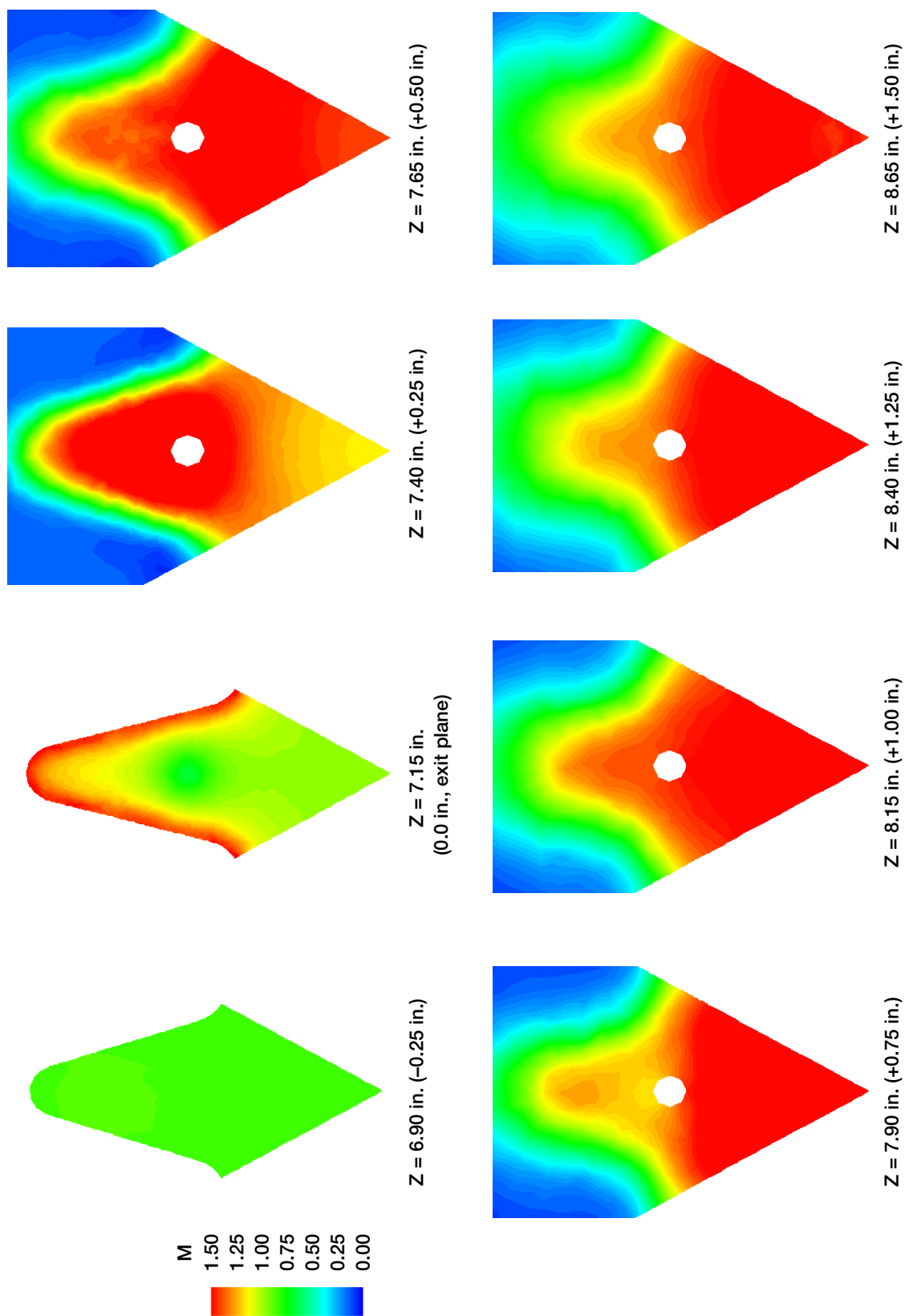Z = 8.40 in. (+1.25 in.)

Z = 8.65 in. (+1.50 in.)

Figure 37.—Axial slices of mach number M contour through lobed diffuser-mixer from 0.25 in. upstream to 1.50 in. downstream of exit plane. With pitot probe offset 0.75 in. from duct centerline.

References

1. Roquemore, W.M., et al.: Trapped Vortex Combustor Concept for Gas Turbine Engines. AIAA Paper 2001–0483, 2001.
2. Burrus, D.L., et al.: Performance Assessment of a Prototype Trapped Vortex Combustor Concept for Gas Turbine Application. ASME Paper 2001–GT–0087, 2001.
3. Hendricks, R.C., et al.: Experimental and Computational Study of Trapped Vortex Combustor Sector Rig With High-Speed Diffuser Flow. Int. J. Rotat. Mach., vol. 7, no. 6, 2001, pp. 375–385.
4. Ryder, Robert C., Jr.; and McDivitt, Timothy: Application of the National Combustion Code Towards Industrial Gas Fired Heaters. AIAA Paper 2000–0456, 2000.
5. Beckwith, Thomas G.; Marangoni, Roy D.; and Lienhard V, John H.: Mechanical Measurements. Fifth ed., Addison-Wesley, Reading MA, 1993.

REPORT DOCUMENTATION PAGE

Public reporting burden for this collection of information is estimated to average 1 hour per response, including the time for reviewing instructions, searching existing data sources, gathering and maintaining the data needed, and completing and reviewing the collection of information. Send comments regarding this burden estimate or any other aspect of this collection of information, including suggestions for reducing this burden, to Washington Headquarters Services, Directorate for Information Operations and Reports, 1215 Jefferson Davis Highway, Suite 1204, Arlington, VA 22202-4302, and to the Office of Management and Budget, Paperwork Reduction Project (0704-0188), Washington, DC 20503.

1. AGENCY USE ONLY (Leave blank)	2. REPORT DATE	3. REPORT TYPE AND DATES COVERED
	July 2002	Technical Memorandum

4. TITLE AND SUBTITLE

Measurement and Computation of Supersonic Flow in a Lobed Diffuser-Mixer for Trapped Vortex Combustors

5. FUNDING NUMBERS

WU–910–30–11-00

6. AUTHOR(S)

Andreja Brankovic, Robert C. Ryder, Jr., Robert C. Hendricks, Nan-Suey Liu, John R. Gallagher, Dale T. Shouse, W. Melvyn Roquemore, Clayton S. Cooper, David L. Burrus, and John A. Hendricks

7. PERFORMING ORGANIZATION NAME(S) AND ADDRESS(ES)

National Aeronautics and Space Administration
John H. Glenn Research Center at Lewis Field
Cleveland, Ohio 44135–3191

8. PERFORMING ORGANIZATION REPORT NUMBER

E–12861

9. SPONSORING/MONITORING AGENCY NAME(S) AND ADDRESS(ES)

National Aeronautics and Space Administration
Washington, DC 20546–0001

10. SPONSORING/MONITORING AGENCY REPORT NUMBER

NASA TM—2002-211127

11. SUPPLEMENTARY NOTES

12a. DISTRIBUTION/AVAILABILITY STATEMENT

Unclassified - Unlimited
Subject Categories: 07, 28, and 34   Distribution: Nonstandard

Available electronically at http://gltrs.grc.nasa.gov/GLTRS

This publication is available from the NASA Center for AeroSpace Information, 301–621–0390.

12b. DISTRIBUTION CODE

13. ABSTRACT (Maximum 200 words)

The trapped vortex combustor (TVC) pioneered by Air Force Research Laboratories (AFRL) is under consideration as an alternative to conventional gas turbine combustors. The TVC has demonstrated excellent operational characteristics such as high combustion efficiency, low NO_x emissions, effective flame stabilization, excellent high-altitude relight capability, and operation in the lean-burn or rich burn-quick quench-lean burn (RQL) modes of combustion. It also has excellent potential for lowering the engine combustor weight. This performance at low to moderate combustor mach numbers has stimulated interest in its ability to operate at higher combustion mach number, and for aerospace, this implies potentially higher flight mach numbers. To this end, a lobed diffuser-mixer that enhances the fuel-air mixing in the TVC combustor core was designed and evaluated, with special attention paid to the potential shock system entering the combustor core. For the present investigation, the lobed diffuser-mixer combustor rig is in a full annular configuration featuring sixfold symmetry among the lobes, symmetry within each lobe, and plain parallel, symmetric incident flow. During hardware cold-flow testing, significant discrepancies were found between computed and measured values for the pitot-probe-averaged static pressure profiles at the lobe exit plane. Computational fluid dynamics (CFD) simulations were initiated to determine whether the static pressure probe was causing high local flow-field disturbances in the supersonic flow exiting the diffuser-mixer and whether shock wave impingement on the pitot probe tip, pressure ports, or surface was the cause of the discrepancies. Simulations were performed with and without the pitot probe present in the modeling. A comparison of static pressure profiles without the probe showed that static pressure was off by nearly a factor of 2 over much of the radial profile, even when taking into account potential axial displacement of the probe by up to 0.25 in. (0.64 cm). Including the pitot probe in the CFD modeling and data interpretation lead to good agreement between measurement and prediction. Graphical inspection of the results showed that the shock waves impinging on the probe surface were highly nonuniform, with static pressure varying circumferentially among the pressure ports by over 10 percent in some cases. As part of the measurement methodology, such measurements should be routinely supplemented with CFD analyses that include the pitot probe as part of the flow-path geometry.

14. SUBJECT TERMS

Combustor; Lobe mixer; Supersonic flow; Pitot tube

15. NUMBER OF PAGES
47

16. PRICE CODE

17. SECURITY CLASSIFICATION OF REPORT	18. SECURITY CLASSIFICATION OF THIS PAGE	19. SECURITY CLASSIFICATION OF ABSTRACT	20. LIMITATION OF ABSTRACT
Unclassified	Unclassified	Unclassified	